Hindawi Publishing Corporation
Journal of Polymers
Volume 2015, Article ID 620362, 24 pages
http://dx.doi.org/10.1155/2015/620362

Research Article

Understanding the Morphological Changes in the Polypropylene/Polyamide 6 Fifty/Fifty Blends by Interfacial Modifiers Based on Grafted Atactic Polypropylenes: Microscopic, Mechanical, and Thermal Characterization

E. P. Collar, J. Taranco, S. Areso, and Jesús María García-Martínez

Grupo de Ingeniería de Polímeros, Instituto de Ciencia y Tecnología de Polímeros, CSIC, C/Juan de la Cierva 3, 28006 Madrid, Spain

Correspondence should be addressed to E. P. Collar; ecollar@ictp.csic.es

Received 4 May 2015; Revised 12 August 2015; Accepted 23 August 2015

Academic Editor: Zhong-Ming Li

The main aim of the present work is to correlate the morphological changes observed in the modified PP/PA6 fifty/fifty blends molded at confined flow conditions with both their mechanical and thermal properties and the kind and the amount of the interfacial modifiers used. Both transmitted light optical microscopy in the positive phase contrast mode, PC TOM, and field emission scanning electronic microscopy, FE SEM, were the used techniques for, respectively, general morphology overview and fractures surface analysis. The interfacial modifiers, a succinic anhydride, aPP-SA, and a succinyl-fluorescein, aPP-SF/SA, grafted atactic polypropylenes obtained and well characterized in authors' laboratories came from the chemical modification of an atactic polypropylene industrial by-product. The amounts of any of both the interfacial modifiers came coded by the Box-Wilson experiment design methodology applied to the overall PP/PA6 binary system, watching that the interfacial agent was not a third component on a ternary blend but a true interfacial modifier in a binary one. All the studies were carried out over suitable specimens according to each test procedure with no further material manipulations to preserve at any moment the morphology of the blends as they emerge from the compression molding step at confined flow conditions.

1. Introduction

From the last century end, both the benefits in costs and the environmental and sustainability requirements, which mean Ecobalance, empowered the reorientation of R&D on new organic based materials. Both, on the one hand, the chemical modification of the known thermoplastic polymers and, on the other hand, the enhancement of the melt blending technologies emerged as key research lines looking at the future [1] more than looking for new organic polymers obtained through expensive and noncompetitive routes of synthesis. Furthermore, from last eighties the strong environmental and sustainability requirements demand the most efficient ways to recover and to recycle industrial plastic waste materials, which in many times appear just commingled. Besides, to satisfy the friendly environment requirements and the right choice of the main constituents, the key parameter on whatever the kind of heterogeneous materials based on thermoplastic polymers is the optimal and well-controlled interfacial interaction level between the components [2, 3]. It means the control over the emerging morphologies on processing operations that remains as an open challenge nowadays [4].

Polyolefin based materials and especially those based on polypropylene, due to their large versatility and competitiveness in costs, are a hot topic either in engineering or in the commodity polymer fields [5] in very different and strategic applications dealing with health, energy, or transport. Drug release and biocompatibility [6, 7], adhesion [8, 9], gas barrier properties [10, 11], flame resistance [12–14], membrane

processes [15], fuel cells, lightest but strongest materials [16], optical properties and thermal stability [17], and commingled plastic waste recycling [18] are just a few examples where necessary are the new nanostructured materials based on polypropylene [19, 20].

The nanotechnology challenge needs properly nanostructured materials able to match macroscopic response levels commanded by interactions at the molecular scales or involving just a few of atoms. On the development of heterogeneous materials based on the organic thermoplastic polymers, it should mean a full control on tailoring the interfacial regions between whatever couple of significant phases. The interfacial ply approach [4] defines the interface as the spatial planar projection of any sensitive specific property from each one of both bordering phases all along the overall interfacial volume that implies a finite thickness region, which strongly influence or even determine the macroscopic behavior of the material [5, 21, 22].

The very different morphologies that can emerge from the blending and molding processes of the thermoplastic organic polymer based materials make it very difficult to get the physicochemical tailoring of the interphases. The troubles extend along the scale-up operations and to all the manufacture process of parts and semifinished goods based on thermoplastic copolymers [23, 24]. Moreover, if as usual the dimensions of runners, gates, dies, and cavities are of the same order of those emerging coarse morphologies, the close proximity to the walls and the flowing dispersed domains induce wall effects by border layer considerations, which could be part of the problem or part of the solution to tailor made morphologies. Current simulation software well solves new models of complex molding processes like multilayer films, sheets, or complex parts but fails to match the morphologies developed in the bulk of the heterogeneous material which in turn determine its performance [25].

Otherwise the bottom-up simulation models starting on the molecular dynamics and atomistic scales cannot cover, at present day, the disparity of 12 orders of magnitude that separates them from the macroscopic ones where the polymeric materials work nor the nine up to the interfacial interactions domain [5]. Therefore, the challenge to forecast the flow-induced morphologies, generated in immiscible polymer blends under the fast, nonisothermal, and high stress conditions flows, characterizing the different processing operations of thermoplastic polymer materials, remains open and needs new modeling tools and new data base [26].

The present work continues the preliminary studies of the effect of both kinds of the grafted atactic polypropylenes obtained at the Polymer Engineering Group's labs under its chemical modification of polyolefins research line [27–38] as efficient reactive interfacial modifiers of the PP/PA6 binary system [39–41]. The study deals with the microscopy and FT-IR spectroscopy analyses of the fifty/fifty blend with modified interface by different amounts of either aPP-SA or aPP-SF/SA grafted polypropylenes and their correlation with their respective mechanical and thermal behaviors. The dynamic mechanical analysis on tensile and shear modes of the pristine and the modified blends and the structural analysis of the crystalline phases of both the PP and the PA6 blend components by synchrotron radiation would be the subject of the next papers [42, 43]. New incoming works will extend the statistic microscopy analyses to the overall compositional ratio of the modified PP/PA6 binary system, well let support by the Box-Wilson experiment design methodology to build up the morphology maps of the PP/PA6 binary system with modified interface molded at confined flow conditions after a reactive processing step.

Indeed, one of the most efficient ways to give rise to stable morphologies is that the interfacial modifiers were able to yield an optimal number of primary bonds across the interphase between main domains [44, 45]. Such primary bonds could avoid postreactive processing coalescence processes and the coarsening of the former well-dispersed domains on further new shear and thermal fields imposed on the heterogeneous system. Moreover, by reducing the sensitivities of such nanostructured materials to the surrounding environments, the interfacial modifiers should ensure the integrity of the materials not only in use but also in storage [46, 47].

From an applied perspective, the polyamide/polyolefin binary systems have been a study matter for several years because of their potential in many industrial applications, mostly related to the decrease in the water absorption of polyamides by blending with polyolefins and the improvements in their impact resistance [48–52, 52–63].

The authors chose the PP/PA6 binary system, as representative of those heterogeneous materials based on polypropylene, where both components are deformable under heat and pressure to study how to modify its morphology by interfacial agents all along the compositional range, aided by the Box-Wilson experiment design methodology [64]. After the preliminary modellization of frame works [39, 40] and of the isothermal crystallization behavior of the propylene matrix [41], the fifty/fifty blend is separately studied in present work in the light of the obtained results and because of its nearness to the inversion phase point as discussed by many authors in literature [49, 52, 53, 61–63].

About the two interfacial agents considered, both based on an atactic polypropylene by-product of industrial reactors and chemically modified by grafting of polar groups would match the requirements of the surfactant substances, with long sequences of nonpolar or aliphatic species, chemically anchored to polar groups [54, 55], which in turn also apply to the development of nanocomposites [5, 56, 58].

2. Experimental

2.1. Materials. Homopolymers used in the present work were two commercial grades: Ultramid B3, nylon 6, supplied by BASF (Spain), and Isplen 050, polypropylene, from Repsol Química (Spain). Table 1 compiles some physical properties of both homopolymers, PP and PA6. The two batch solution modified atactic polypropylenes used as interfacial agents in PP/PA6 fifty/fifty blend were succinic anhydride, aPP-SA, containing 3.05% (wt/wt) of grafted groups, and succinyl-fluorescein, aPP-SF/SA, with 6.2% of attached groups (expressed as succinic anhydride units) [31–33]. Both grafted polypropylenes were obtained at the authors' laboratories by chemical modification of an atactic polypropylene

Table 1: Physical properties of raw materials used in this work.

Polymer	Molecular weight (SEC)		HI	Density	T_m	T_g	%
	$M_w \cdot 10^{-3}$	$M_n \cdot 10^{-3}$	(M_w/M_n)	(gr/cm^3)	(°C)	(°C)	H_2O
PP Isplen 050	334.4	59.0	5.62	0.9	165	−13	<0.2
PA6 Ultramid B3	25.0	13.0	1.92	1.13	221	65	10
aPP Industrial by-product	54.0	2.7	20.0	0.85	NA	−22.4	<0.2

(Table 1) by-product of industrial propylene polymerization reactors supplied by Repsol Química (Spain).

The reaction conditions [30, 31, 34, 35] and the grafted polypropylenes characterization [36–38] were published elsewhere. Figure 1 shows the chemical structures of both aPP-SA and aPP-SF/SA interfacial modifiers, while Table 2 compiles some of their characteristic properties and of the pristine atactic polypropylene, aPP.

2.2. Processing. The studied blends were PP/PA6 fifty/fifty blend and those with modified interphases by the presence of 0.5, 9, or 17.5 w/w percent of aPP-SA or aPP-SF/SA. Prior to the mixing step, polyamide remained at 60°C in an oven for 48 hours to remove the absorbed water. Each dry blend was batch mixing for five minutes at constant torque on a Rheomix 600 chamber attached to a Rheocord 90 Series from Haake (Spain) working at 240°C and 45 rpm. On recovering, each reactive blend remained sunk on an ice bath for cooling and then dried and was pelletized. After an overnight in a vacuum oven, the material was ready for the molding step.

About 3 g of pellets of each blend was compression-molded by a laboratory Dr. Collin Press, (Spain) onto circular sheets of around 20 cm diameter and 100-micrometer thickness. Once at the hot press, the closed mould stays four minutes at the set temperature of 270°C to favor the material melting. Then and after a minute under a pressure of 10 MPa, the closed mould passed to the cooling cartridge under a packing pressure of 20 MPa to reach the room temperature.

2.3. Analysis and Characterization Procedures. Samples for optical microscopy on the light transmission mode, TOM, came from the compression-molded sheets cut as small pieces of around 8 × 5 mm and 100 mm of average thickness parallel to the radial flow direction. Natural Canada balsam attached them to the standard glass cover/slide sample holders. A Zeiss-Jena (Spain) optical microscope, Jenaval model with modified stand for both reflection and transmission modes, was used. Positive phase contrast, P PC, combined with modulated contrast, MC, at the image side was the observation technique adopted because of the different refraction indexes of PP and PA6 homopolymers. Images were taken by a Nikon digital camera (Spain), Coolpix model, attached to the microscope and to the image analysis software Q 500MC from Leica Systems (Spain). All the TOM images were taken at a magnification level of 250x because of the high thickness of the samples otherwise engaged with the mechanical and thermal test requirements.

Table 2: Characteristic properties of the pristine aPP and of the interfacial modifiers used in this work.

Polymer	$M_v^{\text{Grafted}}/M_v^{\text{a-PP}}$	Graft (%)	T_g (°C)
aPP	1.00	0.0	−22.4
aPP-SA	1.20	3.0	−16.5
aPP-SF/SA	1.25	6.2	−15.4

The FT-IR spectra of both the interfacial modifiers and the different blends were recorded on a Perkin-Elmer, Spectrum One spectrometer, working at an average of scans of 32 and a resolution of 4 cm^{-1}. Blend samples just came from the compression-molded films, while powders of the interfacial modifiers were prepared as KBr pellets on 1/170, aPP-X/KBr w/w ratio [37].

Mechanical testing of pristine and the modified PP/PA6 fifty/fifty blends was carried out at room temperature under normal stress regime, on the tensile mode following the UNE-EN ISO 527-3 standards, by an Instron dynamometer (Spain), model 4204, equipped with a high-resolution digital extensometer. Dumbbell specimens of 35 × 2 × t mm, with t = 100 ± 10 micrometers, were cut off the compression-molded sheets in the circumferential sense by using a standardized die attached to a manual press, both from Adamel Lomarghi (Spain). Ten dumbbell specimens for each blend were tested at a crosshead speed of 1 mm/min determining the mean values of the tensile strength (MPa) and strain (%) both at the yield and at the break points. Elastic modulus values showed a high lack of fit into the Box-Wilson models probably because of the small specimen size and the high noise level associated with the measurements and as consequence were out of discussion [39].

The fracture surfaces of the tensile tested specimens were FE SEM observed by a 30 kV field emission scanning electronic microscope, Jeol (Spain), JSM-6335F model. Previously the samples once fixed on standard cylindrical brass holders were gold coated by an Emitech (Spain) sputter coater, K 550X model.

Differential scanning experiments were performed by following a dynamic experimental run under nitrogen atmosphere, on a Perkin Elmer DSC7 (Madrid, Spain) Unix system, indium (T_m = 165.51°C; ΔH_m = 28.45 J·g^{-1}) and zinc (T_m = 419.51°C; ΔH_m = 108.4 J·g^{-1}) calibrated. Standardized aluminum DSC crucibles were filled with around 10 mg of each sample as five piled round specimens, 5 mm diameter

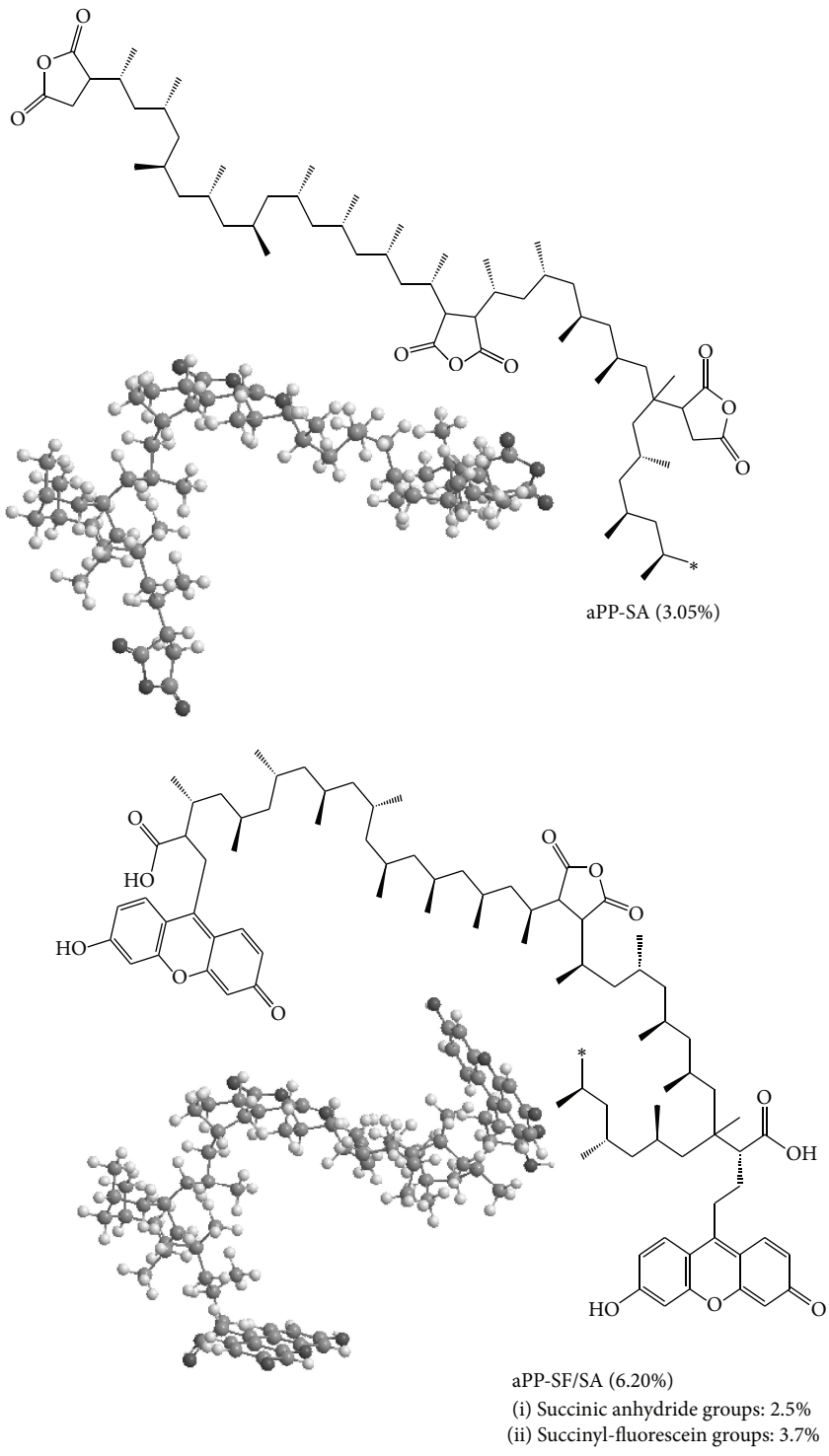

Figure 1: Interfacial modifiers structures.

and 100-micron average thickness, machined by hole puncher from the compression-molded sheets. Each dynamic experimental run consisted of three steps, heating/cooling/heating, at 10°C·min^{-1} from 50°C to 250°C, the first one; from 250°C up to 50°C, the second one (after five minutes keep the sample in the molten state); and newly from 50°C to 250°C, the third one. Both the crystallization-exothermic and the melting-endothermic peaks corresponding to the respective first-order transitions of each one of the two semicrystalline homopolymers, PP and PA6, were recorded. From the peak areas once normalized according to the respective PP and PA6 amounts on each blend [40] and by taking 209 J·g^{-1} and

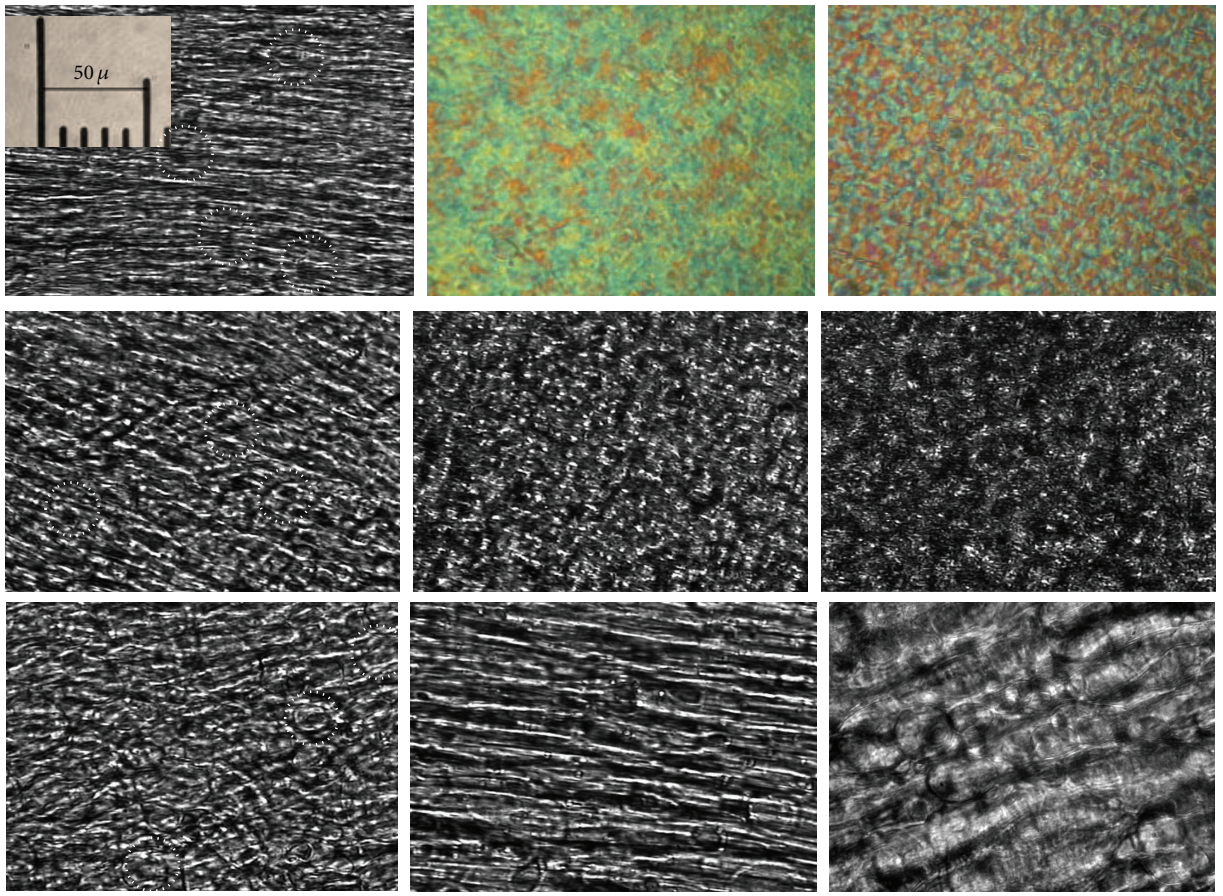

Figure 2: Micrographs 250x by Phase Contrast Transmission Optical Microscopy, PC TOM, of the PP/PA6 fifty/fifty blends: pristine, top row; both from left to right: 0.51%, 9%, and 17.5% aPP-SA, middle row; or aPP-SF/SA, bottom row, modified ones. Top row colour micrographs: cross polarisers, TOM images of the PP and the PA6 homopolymers.

190 $J \cdot g^{-1}$ for, respectively, full crystalline PP and PA6 [65], we calculate the respective crystalline contents for each of both components.

3. Results and Discussion

Tables 3 and 4 compile the tensile strength and strain values of PP/PA6 fifty/fifty blend when, respectively, modified by aPP-SA or aPP-SF/SA. Both include the tensile strength and strain values for both the homopolymers and the pristine PP/PA6 fifty/fifty blend. Table 5 displays the peak temperatures and specific heats of PP and PA6 homopolymers associated with the corresponding heating and cooling scans, while Tables 6 and 7 compile those values for PP and PA6 in, respectively, aPP-SA and aPP-SF/SA modified blends. Therefore, Tables 6(a) and 6(b) show the specific heat values and peak temperatures, respectively, for the isotactic polypropylene, PP, and PA6 in aPP-SA modified blends and Tables 7(a) and 7(b) in aPP-SF/SA modified ones. These experimental values belong to the set of input values fit by following the Box-Wilson methodology, which together with the corresponding ANOVAs were fully discussed elsewhere [39, 40]. The fitted curves for the modified PP/PA6, fifty/fifty modified blends feedback the present work.

Table 3: Experimental values of the tensile test parameters of aPP-SA modified PP/PA6 fifty/fifty blend [the values of both the two homopolymers and the pristine blend are included too].

w/w PP/aPP-SA (%)	Yield point		Break point	
	Strength (MPa)	Strain (%)	Strength (MPa)	Strain (%)
100/0	26.0	9.5	17.3	>473.5
50/0	9.4	0.7	9.3	1.5
50/0.51	5.4	0.7	5.4	1.8
50/9.0	15.0	0.9	17.2	1.9
50/17.5	14.5	0.8	17.5	2.3
0/0	51.3	18.7	49.9	220.8

3.1. Optical Microscopy of the Fifty/Fifty PP/PA6 Blends. As described under Experimental section, samples for the TOM studies were of around 100-micrometer thickness taken from the compression-molded sheets, being virtually identical to those other mechanical and thermal and any other characterization tests. The middle and right hand color micrographs at the top row in Figure 2 correspond to representative observations, 250x, under polarized light and cross polarizer,

Table 4: Experimental values of the tensile test parameters of aPP-SF/SA modified PP/PA6 fifty/fifty blend [the values of both the two homopolymers and the pristine blend are included too].

w/w PP/aPP-SF/SA (%)	Yield point		Break point	
	Strength (MPa)	Strain (%)	Strength (MPa)	Strain (%)
100/0	26.0	9.5	17.3	>473.5
50/0	9.4	0.7	9.3	1.5
50/0.51	12.3	1.3	12.3	1.6
50/9.0	17.0	1.3	17.3	1.4
50/17.5	11.9	0.9	10.5	2.9
0/0	51.3	18.7	49.9	220.8

Table 5: Peak temperatures and specific heat values for the PP and the PA6 homopolymers and in the fifty/fifty blend.

PP/PA	T_{1m} (°C)	ΔH_{1m} (J/g)	T_c (°C)	$-\Delta H_c$ (J/g)	T_{2m} (°C)	ΔH_{2m} (J/g)
100/0	162.2	84.8	110.2	95.5	158.4	91.4
50/50						
PP	161.1	77.40	112.4	87.36	158.10	78.96
PA	218.5	58.22	185.4	54.25	218.4	48.89
0/100	220.5	64.5	178.6	58.5	219.3	54.8

Table 6: (a) Isotactic polypropylene, PP: specific heats and peak temperatures in the PP/PA6 fifty/fifty aPP-SA modified blends. (b) Polyamide 6, PA6: specific heats and peak temperatures in the PP/PA6 fifty/fifty aPP-SA modified blends.

(a)

PP/aPP-SA (%)	T_{1m} (°C)	ΔH_{1m} (J/g)	T_c (°C)	$-\Delta H_c$ (J/g)	T_{2m} (°C)	ΔH_{2m} (J/g)
50/0.51	161.3	90.90	116.8	103.61	159.9	96.11
50/9.00	161.0	77.11	114.4	84.80	158.0	77.71
50/17.49	161.2	70.37	112.3	79.40	155.7	70.64

(b)

PP/aPP-SA (%)	T_{1m} (°C)	ΔH_{1m} (J/g)	T_c (°C)	$-\Delta H_c$ (J/g)	T_{2m} (°C)	ΔH_{2m} (J/g)
50/0.51	218.6	53.48	185.4	49.56	218.6	42.89
50/9.00	218.0	63.56	182.6	46.19	218.3	51.94
50/17.49	217.9	58.01	182.5	48.76	217.5	49.44

Table 7: (a) Isotactic polypropylene, PP: specific heats and peak temperatures in the PP/PA6 fifty/fifty aPP-SF/SA modified blends. (b) Polyamide 6, PA6: specific heats and peak temperatures in the PP/PA6 fifty/fifty aPP-SF/SA modified blends.

(a)

PP/aPP-SF/SA (%)	T_{1m} (°C)	ΔH_{1m} (J/g)	T_c (°C)	$-\Delta H_c$ (J/g)	T_{2m} (°C)	ΔH_{2m} (J/g)
50/0.51	161.5	84.15	115.9	99.60	159.2	86.60
50/9.00	160.6	71.84	114.2	85.55	157.4	72.64
50/17.49	160.6	72.84	111.4	84.58	156.2	74.69

(b)

PP/aPP-SF/SA (%)	T_{1m} (°C)	ΔH_{1m} (J/g)	T_c (°C)	$-\Delta H_c$ (J/g)	T_{2m} (°C)	ΔH_{2m} (J/g)
50/0.51	218.6	52.85	185.8	48.75	218.5	41.26
50/9.00	217.4	58.09	183.8	56.77	217.4	47.75
50/17.49	217.1	56.73	182.4	55.23	217.1	48.50

of both, respectively, PP and PA6 homopolymers studied in present work. Distorted color images on both micrographs are characteristic patterns of the changing pathways of the polarized visible beam with either the three-dimensional order of the crystalline regions or the different thickness of the phase objects all along the sample thickness, for instance, the impinged spherulitic domains growing in the bulk of the compression-molded sheets. From both images it is obviously seen that, once mixed, both semicrystalline components would not be distinguishable by the polarized light observation mode.

Hence, PP/PA6 binary system was studied under the phase contrast technique which makes use of the differences between the refraction index of both homopolymers and is unaffected by the birefringence phenomena [66, 67]. It reveals under a grey scale mode the edges of the different optical areas on a heterogeneous sample which are darker or clearer than others by a combination of diffraction, scattering, and refraction effects when light passes across the material sample. According to the positive phase contrast, P PC, mode used at present work, the richest PA6 areas, with the higher refractive index, would appear as the darkest, while those whitened areas would be the PP richest ones, because of their lower refractive index. To improve the images clarity, the modulation contrast, MC, technique on the image side was combined with the P PC mode. The MC maximizes the optical gradients across the sample and jointly with a low aperture of the sample side condenser it gets an enhanced visibility of the edges and the three-dimensional character of any feature present on the phase objects.

The different grey scale micrographs displayed in Figure 2 show different morphologies mainly characterized by very different distributions, both in shape and in size, of dark and white and more or less warped domains. The left hand, top row micrograph corresponds to a representative field of the pristine fifty/fifty blend, including an insert with a scale bar of 50 micrometers that applies to all the other images. As it is well known, warping is one of the most frequent evidences of phase segregation during solidification [68–70], appearing as parallel bands or ribbons that indicate the deformation direction imposed on the component domains during the molding step. The black worm-shaped PA6 domains appear twice or three times larger in width than white PP domains, which are between 25 and 50 micrometers in length with much clearer and well-defined borders. It is interesting to

observe some likely rounded features (some of them framed by an insert dotted white circle) placed out of the well-defined equatorial focal plan that appear as object phase with diameters between 15 and 25 micrometers. Such features point out to unbroken spherical domains coming from any coalescence processes and placed on those selected zones along the sample thickness closest to the wall mold.

Both left side micrographs placed at the middle and the bottom rows of Figure 2 correspond to the binary system with modified interface by the presence of just 0.5% of aPP-SA (middle) or aPP-SF/SA (bottom). The former seeming distribution of almost parallel bands of the white ribbon-like domains of PP, two or three times narrower than PA6 worm-shaped black domains, which were observable in the pristine blend, appears on both 0.5% modified blends as a homogeneous distribution of not so parallel white and black worm-shaped domains. Both the black and white domains look almost similar in width and the latter show an improved clarity of their borders within the black PA6 domains distribution. Despite the very low amount of any of the interfacial modifiers, the observed enhanced contrast between the black and the white domains well defined on an overall grey scale background for both modified blends if compared with the pristine one indicates a decrease in the segregation level of the immiscible system.

The aPP-SF/SA modifier, left hand, bottom row micrograph, induces the largest effect, which agrees with the expected increase in the interface thickness as the active moieties volume in the interfacial agent increases [71]. Indeed earlier studies [5, 34, 35] showed that the SA groups grafted onto the aPP-SA by solution processes are on a 2/1 ratio, between both the two as backbone, and end grafted groups; to those others both sides grafted into propylene sequences. So the remaining SA groups grafted onto aPP-SF/SA correspond to both sides grafted onto propylene sequences, hindered to react with resorcinol [31] (Figure 1), while those former as pendant or end grafted SA groups, evolved to respectively, SF pendant, or end grafted groups.

It means that while aPP-SA is able to yield true two-arm diblock PP-PA copolymers in selected sites of the interface by forming the corresponding imide bridges (Figure 3), those remaining sides propylene grafted SA groups in aPP-SF/SA interfacial modifier give rise to three-arm block copolymers at the interface with the largest interfacial volume requirements (Figure 3). In agreement with both the simulation results [72] and experimental findings from other authors [73, 74], it means an increase in the interfacial ply thickness and in turn the subsequent decrease on the overall available interfacial reaction volume. It implies some kind of saturation in the reaction capabilities of aPP-SF/SA and in consequence its ability to reduce the mean particle size of the heterogeneous blend.

Figure 4 comes in support of these considerations. Indeed the plot in Figure 4(a) shows the FT-IR spectra for both aPP-SA and aPP-SF/SA interfacial modifiers and the correspondent difference spectrum, which clearly shows a band around 1777 cm^{-1} assigned to both sides grafted SA groups on the latter.

The plots displayed at Figure 4(b) correspond to the Box-Wilson relative absorbance forecasts for the out of plane flexural deformation at 750 cm^{-1} assigned to the "free" end amine groups of PA6 in the fifty/fifty PP/PA6, aPP-SA or aPP-SF/SA modified blends. Both curves appear below the original value obtained for the nonreactive pristine blend, the relative absorbance values for aPP-SF/SA modified blends being higher than those for the aPP-SA modified ones. Indeed, aPP-SF/SA modified blends show an almost constant relative absorbance value whatever the aPP-SF/SA amount.

In contrast, aPP-SA modified blends plot show a sharp minimum absorbance value at just the lowest aPP-SA amount, which increases as aPP-SA amount does up to the nine percent, remaining almost constant for further increases of the aPP-SA amounts. Such evolutions confirm the proposed saturation effect of both interfacial modifiers at the interfaces, immediate for aPP-SF/SA, and above an optimum amount for aPP-SA.

Coming back to the PC TOM images, besides the enhanced view of those spheroids and ellipsoidal features in aPP-SF/SA modified blend, one may observe their increased sizes especially of the ellipsoidal ones together with a well-defined halo effect around almost all these round-like features. The halo effect appears under the modulated phase contrast when the diffracted light fraction that passes through the phase ring, nearest to the border ring, undergoes retarding when crossing from one phase object to another, indicating a significant increase in the border thickness between them. Both the halo effects and the improved visualization of these phase objects allow concluding a significant improvement in the sliding capabilities between the surfaces of both homopolymers in contact during the reactive mixing step although not enough to make them disappear from the observation field. Moreover, because of the stable imides' bridge formed during the reactive mixing step, it is possible to find in aPP-SF/SA modified blend a fraction of these round-like or ellipsoidal features significantly larger in size than those on the pristine and in the aPP-SA modified ones. It suggests that more than to break up, or coalescence processes during the molding step, the largest interfacial volume requirements of the aPP-SF/SA modifier would favor the slippage between those adjacent flow elements all along both the mixing and the molding processes that means in turn the lowest reaction time between the actives sites at the interface.

Middle micrographs displayed at the second and third rows of Figure 2 show the PC TOM images of PP/PA6 fifty/fifty blends 9% modified by, respectively, aPP-SA and aPP-SF/SA. The 9% aPP-SA modified blend shows a very fine and nonstriated morphology where there are no worm-shaped or ribbon-like shaped white PP domains. No rounded or ellipsoidal features out of the focal plane are observable, neither do halo effects around any of the black PA6, or the white PP domains, which, otherwise, do not show well-defined borders as phase object in sharp contrast with the pristine, or the former 0.5% aPP-SA modified blend.

Meanwhile the PC TOM morphology of 9% aPP-SF/SA modified blend shows a decrease in contrast between the black and the white domains larger than that previously

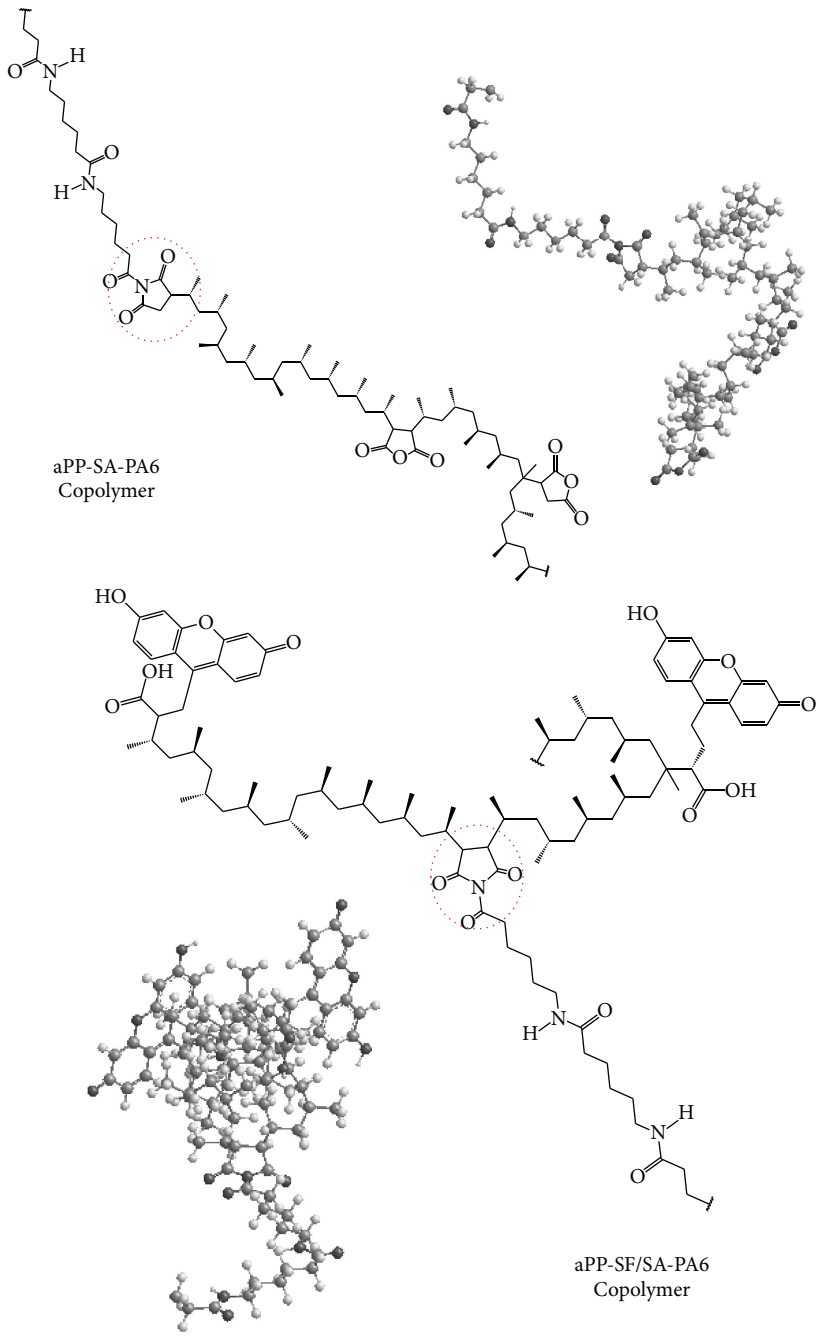

Figure 3: Structure of the two- or three-arm copolymers formed at the PP/PA6 interphase by the chemical reaction between the end amine groups in PA6 and SA groups, respectively, grafted in aPP-SA or in aPP-SF/SA.

observed for the 0.5% modified one, favoring an overall grey scale background. Furthermore, the enhanced visualization of the halo effects around the spheroids and ellipsoidal features is noteworthy, which otherwise appear as larger in size and also in population than in the previously discussed 0.5% aPP-SF/SA modified fifty/fifty blend, and of course in the pristine binary system. From the comparison between the PC TOM morphologies of both 9% aPP-SA or aPP-SF/SA modified blends, it is easy to conclude that each one of them acts in a very different manner in agreement with their structural differences, as discussed above.

A further increase of the interfacial modifiers amount up to 17.5%, right hand images of Figure 2, aPP-SA middle micrograph or aPP-SF/SA bottom one, gives rise to very different morphologies. While the former one displays a kind of fine grain morphology similar to that observed for the 9% aPP-SA modified blend, the latter is showing a coarse grain and striated morphology similar to that observed for the 9%

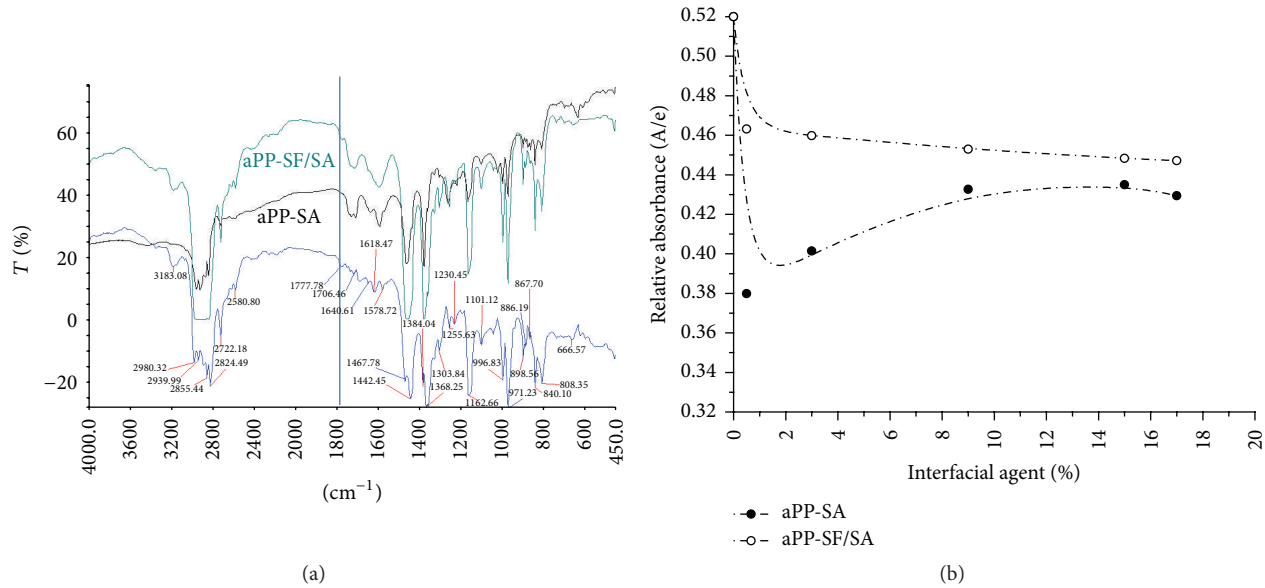

(a) (b)

Figure 4: (a) FT-IR spectra of both interfacial modifiers, aPP-SA and aPP-SF/SA, and their difference spectrum. (b) Box-Wilson forecasts for the FT-IR absorbance band at 750 cm^{-1} (free end amine groups in PA6) in aPP-SA or aPP-SF/SA modified PP/PA6 fifty/fifty blends.

aPP-SF/SA modified blend. A decrease in the heterogeneity of the binary system is common in both 17.5% modified blends, as deduced from the overall image contrast variations that can be appreciated by comparison with their respective 9% modified ones.

The overall dark grey background of the image indicates an increase in the fraction of the incident light that is lost while crossing the sample, because of the absence of abrupt interfacial regions in terms of the differences between the refraction indices of both PP and PA6. It means a decrease in the heterogeneity grade of aPP-SA 17.5% modified blend if compared with the former distribution of well-defined black and white worm-shaped domains that described the morphology of the pristine blend.

Although 17.5% aPP-SF/SA modified blend remains as coarse-grain morphology, its enhanced homogeneity as deduced from the loss of the three-dimensional character of the observed phase objects is worth noting. They appear on a seemingly single focal plane, showing a well-distributed population of grey scale features of which some are halo spheroids, lowest in size if compared with those on 0.5 or 9% aPP-SF/SA modified blends. In addition, the overall and bright grey background of this image indicates the lowest fraction of scattered light that means a blend yielding the highest fraction of transmitted light, on a distorted wave front, unable to define the borders of the different phase objects.

3.2. Tensile Behavior and FE SEM Study of the Fracture Surface of PP/PA6 Fifty/Fifty Blend. As an insert placed at the end-point of the tensile stress/strain curves of the PP, the PA6 and its fifty/fifty blend, Figure 5, three FE SEM panoramic views show their respective tensile fracture surfaces. Tensile fracture always took place along the cross section of the strained specimens, which means that the FE SEM micrographs would inform not only about the fracture process but also about the radial distribution of both components along the specimen cross section.

The top, left hand FE SEM micrograph in Figure 5 shows the representative panorama at 150x of the tensile fracture surface of the PP/PA6 fifty/fifty pristine blend, characterized by two kinds of well-differenced and strained domains, according to the detailed images at 1000x and 2000x as displayed in Figure 6. Some of such strained domains appear as ribbon-like shaped, showing a high level of residual strain after the material breakage. According to the previous PC TOM study, they correspond to the PP domains, highly strained during the molding step. The second domain type corresponds to the big feature almost unstrained placed at the middle of the tensile fracture surface and those others that one may deduce from their footprint left on the sites where they were pulled out during the fracture process. These black worm-shaped PA6 domains as PC TOM observed appear as the largest in thickness and like tip end cylindrical shaped, with their major axis parallel to the radial flow direction. Their dimensions in full agreement with those previously determined by the PC TOM study confirm the confined flow conditions imposed on the emerging morphology of the PP/PA6 fifty/fifty blend.

The micrographs in Figure 6 let us observe the details of the highly strained and finally broken initially ribbon-like polypropylene domains. They seem as a continuous network able to distribute and canalize the initial load applied, by straining, and transmit it to the PA6 domains following a drag mechanism across the PP/PA6 interface [39]. The mechanism should progress at the early load stages, in those thinning middle regions of each PA6 domain, but so less efficiently as to hold off, up to be fully inefficient close to the end tips. Indeed both left hand micrographs at 1000x in Figure 6

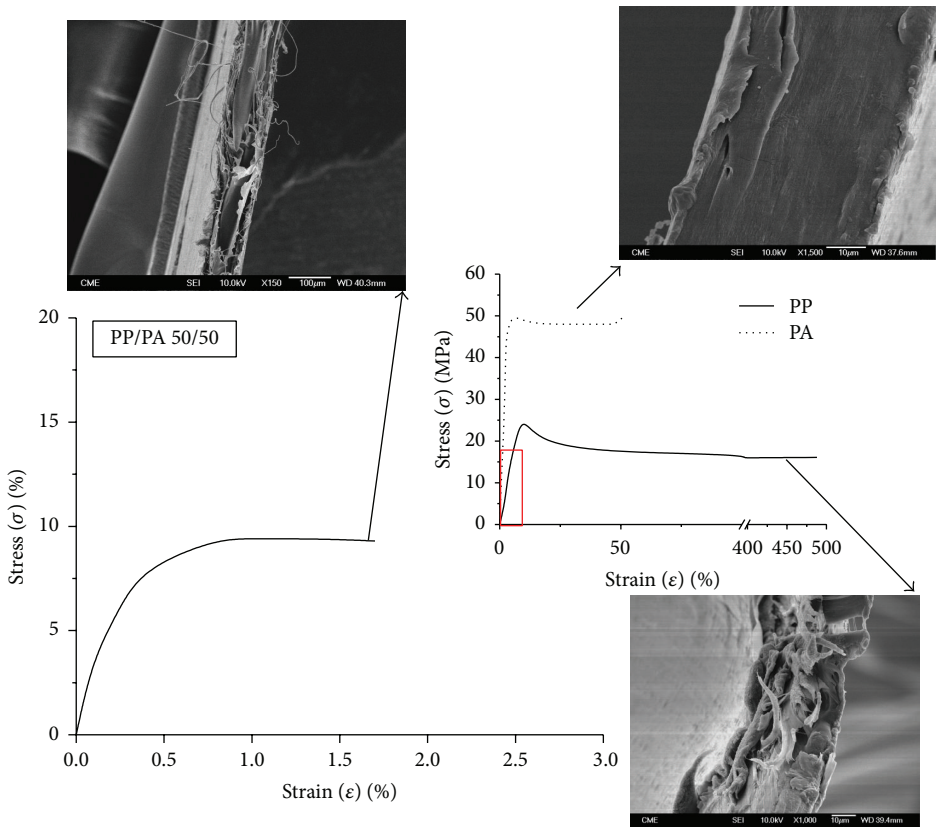

Figure 5: The representative stress/strain curves for the PP and the PA6 homopolymers and the pristine PP/PA6 fifty/fifty blend (red box indicates where the binary system evolves). A FE SEM panorama of each respective tensile fracture surface is included.

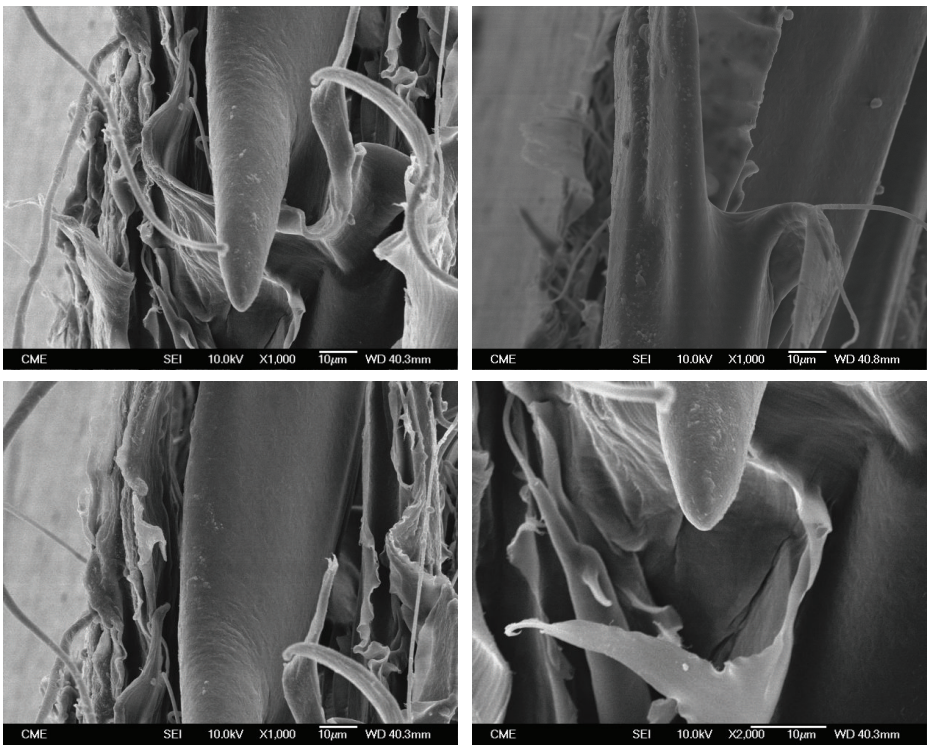

Figure 6: Detailed FE SEM micrographs of the tensile fracture surface of pristine PP/PA6 fifty/fifty blend.

let us observe some small PP protuberances coming from mechanical adhesion points over the large clean and smooth surface of the tip end large PA6 domain, which appears clearly debonded of those highly strained of the PP that imbibed it [39].

These considerations agree with the representative tensile stress/strain plots included in Figure 5, which show the expected sharp decrease in the mechanical parameters of the PP/PA6 fifty/fifty blend if compared with those of each one of the single homopolymers. Neither one of the three strain/stress plots discussed showed any elastic end zone before the end failure that correlates with a low entanglement level in the PP amorphous phase. The fracture surface of the binary system corresponds to a fragile fracture, while the differences in the elongation capability of both homopolymers, and then in their tensile fracture surface, agree with the fact that the temperature test is fifteen degrees above the PP glass transition temperature and more than twenty degrees below that of the PA6 [57].

The tip end PA6 domains observed in the binary system correspond to the highest compliance component that agrees with the assumptions of the mechanical model of the interphase at molecular scale. The fracture surface let us conclude the existence of an interface with nonconstant thickness, higher in the middle than in those end tips, which during flow stabilizes the cylindrical domains against necking, hindering the possibility to obtain finest grain morphology. It would be in those lower thickness areas, acting as stress concentrators, where the separation between domains begins by breaking of the mechanical adhesion points and as it indicates the small protuberances in the micrometer range regularly observed over the PA6 domains. The successive micro void and micro cracking process should end with the catastrophic failure of the material by the overall pullout of a critical number of the PA6 foreign domains, depending on their number and their interdistances. Any efficient interfacial agent should be able to change this situation at least by reducing the particle size of the disperse phase and physical interaction level or furthermore by forming primary bonds on different sites of the interphase.

It is worth mentioning that, on molding at confined flow conditions and because of the different interfacial tension of each component with the metallic surfaces of the mixing device, it is usual that the majority of component forms a melting carcass by covering the metal surface of the mixing elements. The dispersed domains of the minor amount component, coarsely approached to spheroids at the beginning of the mixing process, tend to be deformed into ellipsoids with increasing aspect ratios to form inserted cylinders in the former melting carcass, as its own melting and the overall flow processes progress. As the softest polymer, the polypropylene absorbs most of the plastic deformation energy and although both components reach in turn the molten state, the disperse PA6 domains, as stacked cylinders, may eventually undergo confined compressive deformations in the meantime which reach the full molten state. Such description well explains the FE SEM image of the panorama of the tensile fracture surface of the fifty/fifty blend in Figure 5. As the interfacial area increases, some interfacial flow instabilities by slippage between domains appear, favoring the micro holes formation inside the mixing flow elements of the disperse phase up to a critical threshold, above which the flow elements break into other smaller ones with lower diameters and more or less spheroid geometries. The process may repeat itself, as the external flow conditions, mainly shear and thermal fields, favor the successive average segregation to reach close to the smallest particle size feasible from the combination between the mixing device and the processing conditions imposed.

Inside the mold, and once again the blend into the molten state, one finds that the strangling process of those former overstrained fibres of the dispersed phase that yield a morphology of well-dispersed smaller and nonregular shapes or even droplets of the second component is not always an irreversible process, that is, the particular case when the blend components are two immiscible polymers as the PP and PA6 are. The residual breakup/coalescence balance between the particles of the disperse phase, imposed by the interfacial tension differences between both phases and frozen after cooling, may be liberated under any external stimuli as the temperature/pressure binomial on further processing operations. The corresponding emerging morphology comes defined by its striation thickness distribution and its average striation thickness, as shown in the previous PC TOM image for the pristine blend (Figure 2).

Findings by different authors [46–50] have shown that the viscosity ratio between polypropylene and polyamides does not seem to be so significant in predicting the phase inversion in their blends, concluding that the different particle sizes are sharply depending on the mixing procedures. The capillary rheometer studies for the PP/PA6 binary system carried out in the usual processing temperature range between 230 and 260°C let us confirm that the PP/PA6 binary system shows a negative deviation of the additive rule which agrees with the lack of adhesion at the interphase between both components. Moreover, it is confirmed that the PP viscosity at the shear rates range for extrusion or compression molding below 200 s^{-1} is higher than that of the PA6, which otherwise shows the highest viscosity at shear rates above 1000 s^{-1} as usual, for example, in the injection molding processes.

These rheological considerations come in support that, in the temperature range considered, the former PP domains should tend to break and to disperse the PA6 into lower size domains. In the PP/PA6 fifty/fifty blends and at the magnitude order of the shear rates developed during the molten state stay, first on the mixing chamber and after on the confined flow conditions at the compression molding device, the PP should tend to form the continuous phase because of its higher viscosity. In addition those flow elements of the PP just in contact with the metallic walls on either the mixer or the compression mould would be the most favored to strangle as much as possible the PA6 domains. Far from the mould walls, in the bulk of the molten state, the dispersed PA6 domains should tend to coalesce on both the mixing and the molding devices as flow continues. It explains the pristine blend images coming from the PC TOM and the FE SEM analyses, Figures 2 and 5, respectively.

Thermodynamic considerations say that any stable morphology always must satisfy the condition of hydrostatic equilibrium by which the pressure component normal to the surface of any element must be constant. As the pressure at the interface is nonisotropic, it implies that the generation of a stable morphology requires a continuous change in the transversal components of the diagonal of the pressure tensor at the interface to reach such condition. Since the respective hydrodynamic and interfacial stresses balances at the interface are not in balance, it demands a continuous increase of the interfacial area by a continuous deformation of the dispersed domains from droplets to ellipsoids to almost fibers. If conditions are favorable, that is, enough shear level and viscosity ratio far away of unity, those enlarged domains would break into small droplets. However, the PP/PA6 fifty/fifty blend states a challenge because it shows the more close to one viscosity ratio, because of the minimization of the compositional ratio effect. It means the minimization of the rheological driving forces is able to further increase the interfacial area by domains breakage, obliging to the disperse domains to evolve to less common geometric forms with enlarged surfaces [50]. Extra large aspect ratio fibres and ribbon-like features are the most common shapes which one finds in the pristine fifty/fifty blend images on either the PC TOM, Figure 2, or the FE SEM microscopy, Figure 5.

When the rheological driving force is significant onto the morphology development, several approaches have concluded that the emerging morphology of those combinations of compositional and mixing conditions where the viscosity ratio between the components is close to 1, according to the Weber number expression [2], must be characterized by the minimum particle size of the dispersed phase [49, 50]. For the PP/PA6 binary system, different authors have shown that the mixing procedures, more than the viscosity ratio, are the key factor that determines the obtained morphologies from the early stages of the mixing processes. The complex flow between and around the droplets generates a distribution of viscoelastic stresses both tangential and normal to the interfacial plies, which results to be, respectively, the highest at the equators and the lowest at the tips of the initial spheroids, after ellipsoids, then cylinders, and so on, as the deformation progresses. It explains the progressive thinning of the elongated dispersed domains, which ends in the necessary necking, previous one to the breakage of each one of those initially large disperse domains, into several small others. The FE SEM image of the tensile fracture surface of the pristine blend in Figure 5 and the corresponding tip end details at 1000x and 2000x magnifications displayed in Figure 6 well agree with these considerations.

3.3. PP/PA6 50/50 Modified Blends: Tensile Behavior and FE SEM Study. How an interfacial modifier decreases the interfacial tension between the blend components, giving rise to fine stable morphologies on further processing operations, is a complex subject that, from a mechanistic perspective, is mainly driven for its affinity with the involved phase domains and with the local changes in its concentration all along the interfacial ply. Such variations occur during flow, as the dynamic deformation of those phase domains, initially droplets, their thinning, and subsequent necking processes before breakage, goes ahead. The interfacial agents of low molecular weight tend to concentrate at the tips of the dispersed domains because of the viscoelastic stress concentration in such points, yielding poorly coating regions or even uncoated ones. It results in heterogeneous interfacial tension reductions and the overstretching of the tips because of their locally reduced interfacial tension [50, 58] and explains the higher efficiency of the high molecular weights interfacial modifiers. Otherwise, the existence of such concentration gradients at the interface suggests the existence of optimal amounts of the interfacial modifiers, able to stabilize the flow conditions at the interface from the early stages of any right mixing process. It is convenient to take in mind these considerations on trying to understand the FE SEM panoramic and the detailed images of the tensile fracture surfaces of the 0.5, 9.0, and 17.5% aPP-SA, left hand micrographs, or aPP-SF/SA, right hand ones, modified blends, Figure 7, which show significant morphological differences among them and with respect to the pristine blend.

The top four micrographs set in Figure 7 correspond to the 0.5% aPP-SA, left hand, or the 0.5% aPP-SF/SA, right hand, PP/PA6 fifty/fifty modified blends. Both sides of each specimen more close to the mould walls appear as a PA6 continuous phase from which several high aspect ratio PP filaments highly strained emerge. According to the interfacial agent concentration gradient model previously discussed, just 0.5% of aPP-SA seems to be not enough to full coating of the PA6 domains. Indeed it should remain preferentially concentrated at the tip ends of the PA6 domains. The highest the shear level is, the process would be favored and hence more close to the wall mould; we find after the 2-3-micrometer skin zone a well-defined flow transition zone where PP domains appear as high aspect ratio filaments with diameters below 3 micrometers. Such filaments participated all along the loading process well imbibed in a continuous matrix of PA6; some of them underwent cold-drawn processes, while other ones appear just broken but well bonded to the continuous PA6 domains that imbibed them. In the middle section of the specimen, the core shows the footprint of a large PA6 domain cleanly debonded during the fracture process. In the flow transition zone between the skin and the core, one finds several highly strained worm-shaped PP domains. These observations show a fine correlation with the previous optical microscopy observations.

The right hand upper images of Figure 7 display the morphology of the PP/PA6 fifty/fifty blend modified by 0.5% of aPP-SF/SA that looks very different from that of the 0.5% aPP-SA modified one discussed above, because it does not show any evidence of continuous phase areas of PA6 all along the fracture surface. The decrease in the particle size distribution of the PA6 domains all along the cross section of the specimen, with respect to the pristine blend, agrees with the expected aPP-SF/SA efficiency in the improvement of the interfacial interaction level between the PP and the PA6 because of its higher content on polar moieties than the aPP-SA. After the 2-3 micrometers of skin, one may observe a flow transition zone that extends to almost the core region of the specimen with no evidence of those PA6 debonded domains

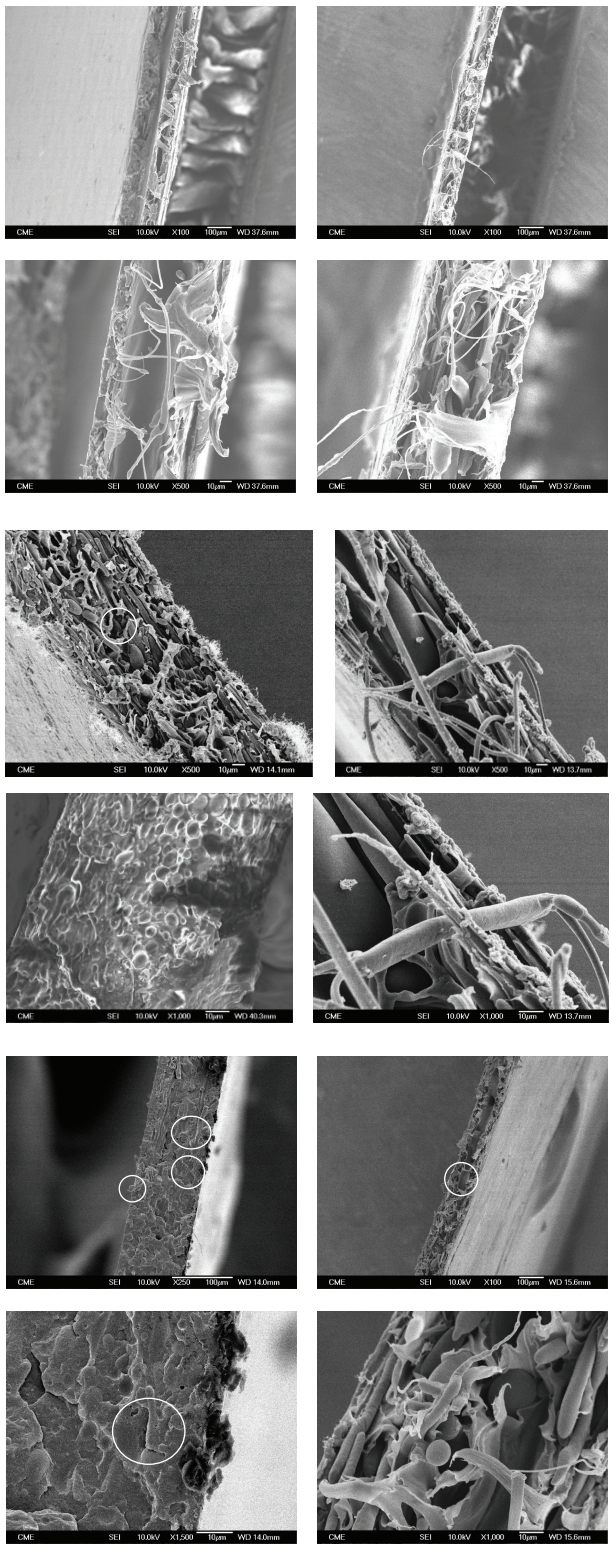

Figure 7: Set of panoramic and detailed FE SEM micrographs of the tensile fracture surface of (from top to bottom) 0.51, 9.0, and 17.5% aPP-SA (left hand) or aPP-SF/SA (right hand) modified PP/PA6 fifty/fifty blends.

that were observable both on the 0.5% aPP-SA modified blend and in the pristine blend. Besides their decrease in size, the shapes of the PA6 domains in the 0.5% aPP-SF/SA modified blend look different, not as cylindrical or ellipsoidal geometries, but as ribbon-like ones. The larger depth of field of the scanning electron microscope allows explaining those black halo rounded features observed by P PC TOM, Figure 2, for this blend and all the other aPP-SF/SA modified blends. They should correspond to the different cross sections of such features, depending on their random orientation and projected as seemingly spheroids over the equatorial plane of the P PC TOM observation field.

Figure 8 displays the representative tensile stress/strain plots of the different PP/PA6 fifty/fifty modified blends, together with a representative FE SEM micrograph of each fracture surface detail. Meanwhile the tensile strain values are very similar in all of them; the above-discussed effect of the lowest amount of the aPP-SA modified blend on its emerging morphology explains its lowest tensile strength values if compared with any of the other five modified blends studied. Sited at the amorphous regions, the primary bonds formed at the interphase would play a key role in the end strain capabilities of the different modified blends. As discussed above, the very small amount of the 0.5% of the aPP-SA and the wall mould effect give rise to a phase inversion effect at such highest shear regions, as that found by other authors [47, 54, 63] for low concentrations of interfacial modifiers, below the 1 percent. Although such small amounts would be efficient to give rise to more thermodynamically stable interfaces and then a smaller interfacial tension, they are not enough to yield the interfacial coating grade necessary to get the optimal reduction of the largest domains.

In the respective middle (9%) and bottom (17.5%) micrographs displayed in Figure 7, one may observe that the PA6 domains of the 9% aPP-SA modified blend appear as the lowest in size and the largest in number of any of the other blends studied.

The 9% aPP-SF/SA modified blend shows big PA6 domains located at the nucleus of the specimen cross section on bordering with the wide transition flow region where the PP domains show a high level of residual deformation. It suggests a well interfacial modifier distribution between the PP and the PA6 domains, giving rise to the progressive size reduction of these later and the maximization of their number. The increase in the magnification level up to 1000x lets us observe the homogeneous distribution all along the cross section of the material of the PA6 dispersed domains well embedded in the highly strained PP network, appearing as the lowest in size of all the modified blends, with radius below 5 micrometers. These kinds of stable morphologies come characterized by thick interfaces of around sixty nanometers or lower between almost spherical domains which assures the minimum interparticle distances between the domains of the disperse phase, but large enough to avoid any coalescence process [41]. These observations show an excellent correlation with the corresponding PC TOM images in Figure 2 where the optimal contrast between the phase objects observed in the 9% aPP-SA modified blend lets us conclude not coarse but indeed fine grain morphology.

The details of the 9% aPP-SF/SA modified blend (middle micrographs set, right hand micrograph, Figure 7) let us observe on the one hand the almost clean skin of the largest PA6 domains and on the other hand some of the highly strained cylindrical or worm-like PP domains, clearly coated by a fine shirt of a foreign material. It looks very similar to that of the small-localized protuberance at the surface of the largest PA6 domain viewed in this micrograph. Furthermore, to act as spatial tracers of the three-arm star copolymer formed during the mixing step, these areas would confirm the proposed saturation effect for the aPP-SF/SA interfacial modifier. It was not achieved by the progressive and homogeneous size reduction of the PA6 domains as it was the case for the 9% of the aPP-SA modified blend, but by the tightening of those former cylindrical or worm-like shaped PA6 domains giving rise to those ribbon-like features displayed on the corresponding detailed micrograph at 500x. The present discussion agrees with the representative stress/strain plots for each of both modified blends, Figure 8, where one may observe the high ductility of the 9% aPP-SA modified blend, with respect to the 9% aPP-SF/SA modified one, and further the low level of elongation at break of this later.

The bottom FE SEM micrographs set in Figure 7 let us appreciate the effect of the increase on almost twice the optimal interfacial agent concentration over the emerging morphologies in the modified PP/PA6 fifty/fifty blends. The lowest magnification micrographs show the panoramic views of both the tensile fracture surfaces for, respectively, the 17.5% aPP-SA modified binary system, left hand micrograph, and the 17.5% aPP-SF/SA modified one, right hand micrograph. While the latter remains as two well-differenced domains' morphology, the former shows a homogeneous contrast of all the features displayed all along the fracture surface just as it was deduced too over the PC TOM image (Figure 2).

The increase in the magnification level for both modified blends up to, respectively, 1500 and 1000x lets us appreciate for the aPP-SA modified blend the tensile fracture surface of a seemingly homogeneous material showing isolated peaks and fibrils below 1 micrometer long as the characteristic features of a ductile failure mechanism (Figure 8). Furthermore, the high coating level of all the homogeneously dispersed features is noteworthy, most of them as spheroids below five micrometers in diameter, coating included, which means in the same size range of those previously observed for the 9% a-PP-SA modified blend, but with a full coating of their surfaces. It explains the representative stress/strain plot of the 17.5% aPP-SA modified blends, Figure 8, which shows a defined yield point, followed by a small region of constant stress elongation, after which appears a well-defined end elastic zone before the failure. The latter agrees with the participation at the end stages of the loading process of those above-mentioned microfilaments between the domains and the continuous matrix, as they appear in the inset 5000x detailed micrograph included in this same plot.

As all the other aPP-SF/SA modified blends, the 17.5% aPP-SF/SA modified one shows two well-differenced domains' morphology but with the lowest in size domains of the dispersed PA6 component, of all the aPP-SF/SA modified

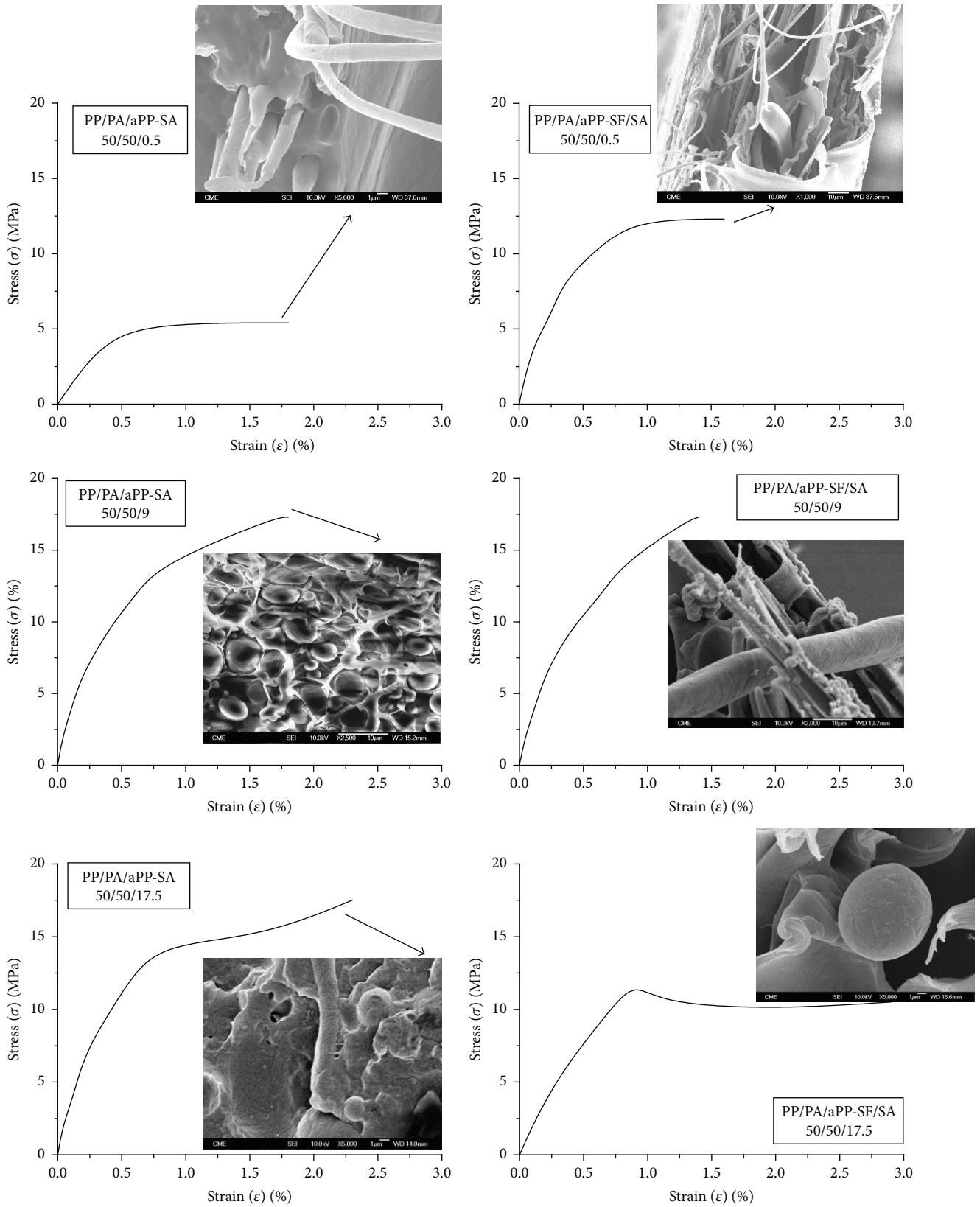

Figure 8: The representative stress/strain curves for the modified PP/PA6 fifty/fifty blends as indicated. On each plot, a detailed FE SEM micrograph of the corresponding tensile fracture surface is included.

blends. One may observe clearly defined three characteristic of the compression-molded materials. An outwards skin zone, below ten micrometers thickness; and a nucleus or core region, characterized by the largest cylindrical PA6 domains together a few rounded ones with diameters around 8 micrometers or below just placed at the imaginary middle axis of the specimen. The third one corresponds to the transition region between both, where most of the PA6 cylindrical or worm-like domains appear as well coated and tip end shaped.

This emerging morphology explains the representative stress/strain plot at the bottom of Figure 8 where not only does a well-differenced yield point appear but even a light stress falls after it, which remains almost constant while the deformation continues, up to the end failure, without any end elastic zone. The inset 5000x detailed micrograph at this plot lets us observe a full-coated spheroid, around 8 micrometers in size, remaining after the end failure, yet attached to one of the highly strained PP domains that embedded it. In such sense, the Box-Wilson forecast [39, 48] that shows the evolution of the tensile test parameters of either the aPP-SA or the aPP-SF/SA modified PP/PA6 fifty/fifty blends appears plotted in Figure 9. The top plot shows both the yield and the break tensile strength evolution, and the bottom one shows the elongation at break. A comparative set of detailed micrographs of the fracture surfaces of both the 17.5% aPP-SA or the aPP-SF/SA modified blends are included illustrating their respective very different morphologies as the main responsible thing in turn of the blend mechanical properties.

Indeed the saturation effect of the aPP-SF/SA-NH-PA6 terpolymer at the lowest aPP-SF/SA content appears well confirmed by the maximum for both the strength and the strain evolution plots at this region. Once above the optimum amount of the 9% as the available interfacial volume, increasing amounts of the aPP-SF/SA show slightly higher yield than break strength values in agreement with the interfacial terpolymer formation and with the absence of an elastic end zone before the failure because of a highly strained but nonductile amorphous phase. It agrees with the displayed morphology in the corresponding detailed micrographs included as well as with the strain values at the highest aPP-SF/SA contents for this fifty/fifty modified blend. Indeed, it almost recovers its maximum strain capabilities; meanwhile the corresponding strength values decrease.

The strain evolution of the aPP-SA modified blends shows an almost constant set of low values even close to the pristine one, up to 9%, while its corresponding strength values significantly grow reaching a maximum at this amount of aPP-SA. This critical point lets us identify the optimum concentration because increasing amounts decrease the strength values to a level below those of the maximum. It is noteworthy that, in the same manner that the aPP-SF/SA modified blends do, the aPP-SA modified ones show different yield than break strength values above the 9%, the latter being the highest. It agrees with the observed morphology and with the existence of a highly strained but now ductile amorphous phase because of the linear structure and then best slip capabilities of the interfacial aPP-SA-NH-PA6 block copolymer [75]. Indeed, detailed tensile fracture surface micrographs of selected zones of both aPP-SA, left hand, and aPP-SF/SA, right hand, 9% modified blends, Figure 10, let us observe several highly strained regions that look as high entanglements of filaments spherical features ended. Their sizes were below five micrometers in diameter and 1.5 micrometers in length, the largest being almost in the nanometer range for the aPP-SA modified sample and even smaller at the aPP-SF/SA modified one. Such long drawn microfilaments morphology [60] appears as typical of the ductile stretching modes on critical sites across the interface on heterogeneous materials.

3.4. PP/PA6 50/50 Modified Blends: Thermal Behavior. Tables 5–7 compile the peak temperatures and specific heat values associated with the dynamic melting and crystallization processes undergone by the PP/PA6 fifty/fifty blends in the DSC oven. The peak temperatures displayed in Table 5 evidence that once in the fifty/fifty blend, both homopolymers undergo an increase in their respective dynamic crystallization temperatures of 2.2°C, the PP, and 6.8°C, the PA6, with respect to their reference values as single homopolymers but molding at the same blending conditions. Moreover, the sensitivity of the compression-molded PP homopolymer, to the pressure absence during the crystallization process in the DSC oven, is noteworthy. It gives rise to a decrease of 3,8°C in the corresponding melting temperature, which falls up to 158.4°C, indicating a poor perfection grade of the monoclinic PP crystals formed under a dynamic crystallization regime [3, 76]. This effect imposed by the processing conditions and indicative of its rightness, remains once the PP in the binary system and, either in the aPP-SA or the aPP-SF/SA modified ones. In contrast but in agreement with the rheological considerations for each of both homopolymers, this effect appears minimized in the compression-molded PA6 homopolymer and indeed absent once in the pristine or in the modified fifty/fifty blends in which the PA6 shows the same melting peak temperature on the first and the second dynamic heating scans.

Tables 8 and 9 show, respectively, the differences between the PP and the PA6 peak temperatures in the aPP-SA or aPP-SF/SA, PP/PA6 fifty/fifty modified blends and their respective in the pristine one. The almost neglectable effect, below 0.5°C, of any of both the interfacial agents over the melting temperatures of the PP in the modified blends as they come from the compression molding process is noteworthy. It also applies to the PA6 in the aPP-SA modified blends. Nevertheless, on both 9 and 17.5% aPP-SF/SA modified blends, the PA6 shows a melting temperature decrease above 1°C with respect to that in the pristine blend. Even this effect appears in the melting temperature of the PA6 coming from the second heating run of these modified blends.

On the modified blends, the PP shows melting peak temperatures coming from the second heating run with significant variations of around 2°C either above or below that of the pristine blend and, respectively, for the lowest and the highest amounts of any of both interfacial modifiers. By the way that the melting peaks of the second heating run overcome from the previous crystallized material, it is noteworthy that the crystallization peak temperatures of both

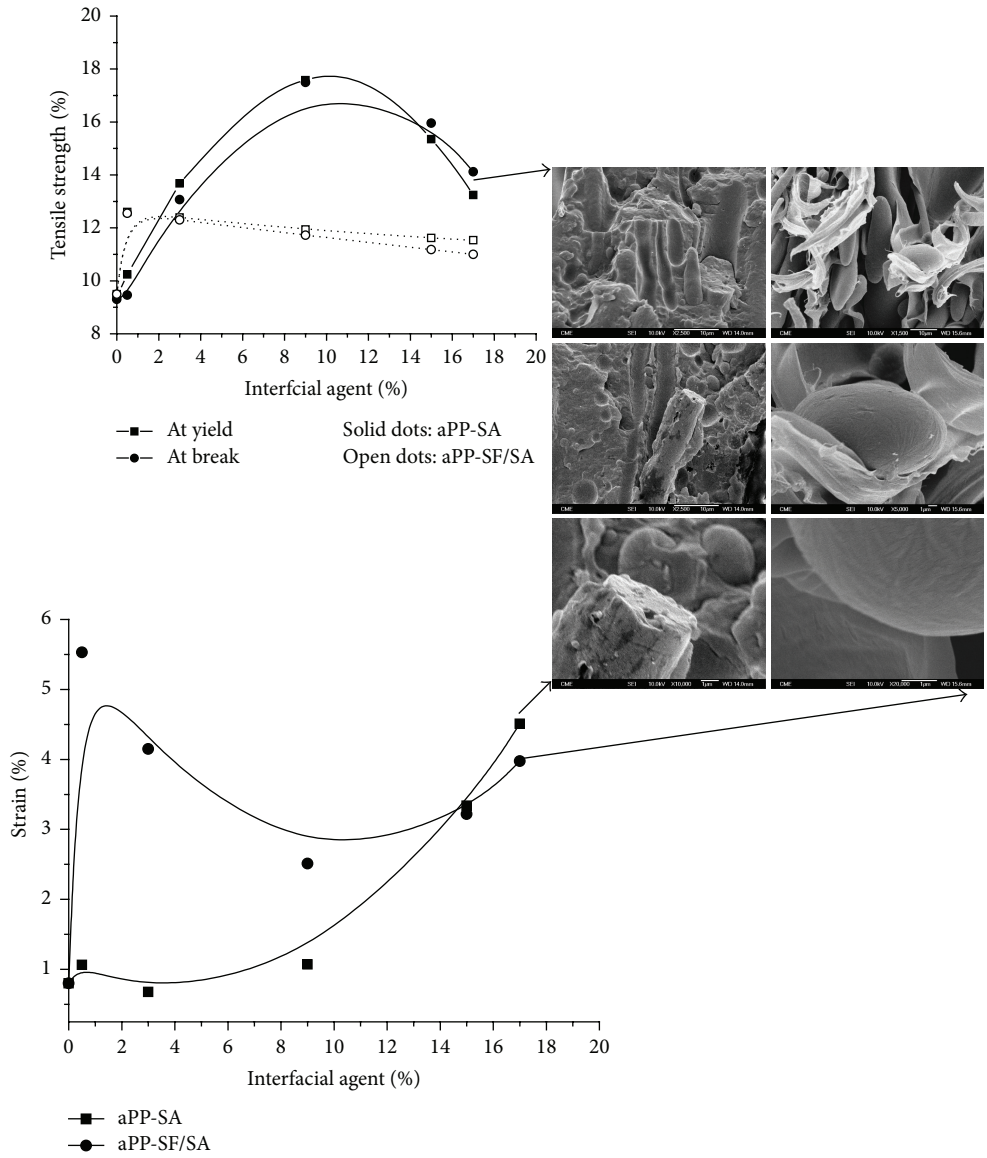

Figure 9: Tensile strength and strain Box-Wilson forecasts for aPP-SA or aPP-SF/SA modified PP/PA6 fifty/fifty blends. High magnification FE SEM micrographs for the blends with the highest amount of the interfacial modifiers are included.

the PP and the PA6 crystalline phases show the highest differences with respect to their respective at the unmodified blend. Indeed, the two highest differences, 4.4°C, Table 8(a), and 3.5°C, Table 9(a), appear for the PP crystalline phase, respectively, in the 0.51% aPP-SA or aPP-SF/SA modified blends. The PA6 crystalline phase needs the highest amount of both interfacial agents to show the largest effect over its crystallization temperatures, almost 3°C below that of the pristine blend, for all the aPP-SA modified blends and for that modified one at the highest content in aPP-SF/SA.

Because of the nucleating effect of the foreign substances, and as the dynamic crystallization temperature correlates with the crystallization rate of a polymer, one finds that both the PP and the PA6 undergo an acceleration in their respective processes when blended at the fifty/fifty w/w ratio. The increases, previously commented on, of 2.2 and 6.8°C for, respectively, the PP and the PA6, with respect to each respective pristine compression-molded homopolymer, confirm this point. All the significant differences of the PA6 peak temperatures in the modified blends appear below the lowest modifier amount and show negative values that mean closer values to these of the PA6 homopolymer than those in the pristine blend. It agrees with the compatibilization effect by the action of any of both aPP-SA and aPP-SF/SA as reactive agents with the PA6 as previously discussed.

The nonreactive nature of any of both interfacial modifiers with respect to the PP implies that only secondary interactions may occur. So one finds that the crystalline phase of the PP at the lowest amount of any of both interfacial agents shows the highest and positive difference of its crystallization temperature, indicating not enough interfacial agent to get an overall improved interaction with the foreign PA6 domains.

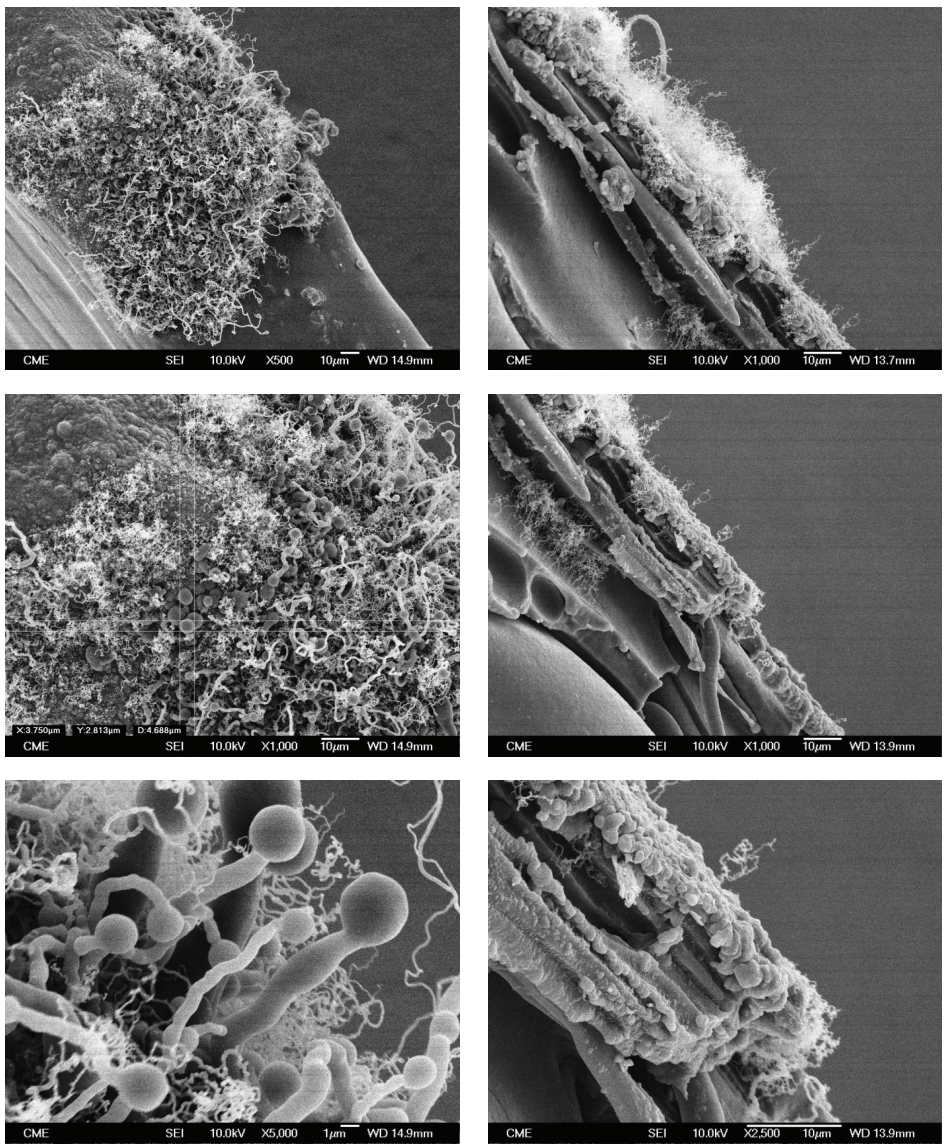

(a) (b)

Figure 10: Detailed FE SEM micrographs of the tensile fracture surface of 9% aPP-SA (a) or 9% aPP-SF/SA (b) modified PP/PA6 fifty/fifty blend showing the filament features associated with ductile fracture processes at the interphase.

As the interfacial modifiers amount increases the dynamic crystallization peak temperatures approach that of the pristine blend and even that of the pristine homopolymer. First results analysis of the isothermal crystallization and WAXS synchrotron experiments, let to correlate these dynamic thermal results with the morphological changes in the PP crystalline superstructure. Indeed, the first analysis [43] shows variations in the long spaced PP values with respect to the unmodified system between 5.8 and 13.0 percent for the aPP-SA modified blends and between 11.0 and 18.2 percent for the aPP-SF/SA modified ones.

As it is well known, fracture always occurs at the amorphous regions of the semicrystalline polymers [36, 40–43]. By definition, it would be at these regions where any amorphous interfacial modifier must be always located. So and on a first approach, it could be interesting to look for any correlation between the role played by the interfacial modifiers and the overall amorphous content of the heterogeneous blend. The Box-Wilson forecasts [40, 48] for the PP and PA6 crystalline contents show a well fitness to calculate by difference their respective amorphous content and then by adding them the overall amorphous content of the modified blends. Therefore, the plots displayed in Figure 11 show the evolution of such crystalline contents as a function of the amount of each of either the aPP-SA or the aPP-SF/SA as interfacial modifiers.

First heating scan plots inform about the role played by the processing history of the modified blends and hence correlate straight forward with their mechanical behavior; indeed both homopolymers are showing the highest crystalline contents as they come from the compression molding

Table 8: (a) Isotactic polypropylene, PP: differences between the peak temperatures of the PP/PA6 fifty/fifty aPP-SA modified blends and their respective ones in the pristine one. (b) Polyamide 6, PA6: differences between the peak temperatures of the PP/PA6 fifty/fifty aPP-SA modified blends and their respective ones in the pristine one.

(a)

PP/aPP-SA (%)	ΔT_{1m} (°C)	ΔT_c (°C)	ΔT_{2m} (°C)
50/0.51	0.2	4.4	1.8
50/9.00	−0.1	2.0	−0.1
50/17.49	0.1	−0.1	−2.4

(b)

PP/aPP-SA (%)	ΔT_{1m} (°C)	ΔT_c (°C)	ΔT_{2m} (°C)
50/0.51	0.1	0.0	0.2
50/9.00	−0.5	−2.8	0.1
50/17.49	−0.6	−2.9	−0.9

Table 9: (a) Isotactic polypropylene, PP: differences between the peak temperatures in the PP/PA6 fifty/fifty aPP-SF/SA modified blends and their respective ones in the pristine one. (b) Polyamide 6, PA6: differences between the peak temperatures of the PP/PA6 fifty/fifty aPP-SF/SA modified blends and their respective ones in the pristine one.

(a)

PP/aPP-SF/SA (%)	ΔT_{1m} (°C)	ΔT_c (°C)	ΔT_{2m} (°C)
50/0.51	0.4	3.5	1.1
50/9.00	−0.5	1.8	−0.7
50/17.49	−0.5	−1.0	−1.9

(b)

PP/aPP-SF/SA (%)	ΔT_{1m} (°C)	ΔT_c (°C)	ΔT_{2m} (°C)
50/0.51	0.1	0.4	0.1
50/9.00	−1.1	−1.6	−1.0
50/17.49	−1.4	−3.0	−1.3

process. The PP, as the lowest melting point component, shows the highest crystalline contents, around 30 to 60 percent above those of the PA6. Further to the previously mentioned nucleation effect of the PA6 over the PP [40, 41], it agrees with the previous rheological considerations about the processing steps, which in turn correlate with the PP role under the tensile testing as previously discussed.

After each blend remains for five minutes in the molten state at the DSC oven, the dynamic and pressure-free cooling process gives rise to an almost parametrical downward shift of the PP crystalline content plot with respect to the previous one discussed coming from the first heating scan. The aPP-SF/SA modified blends show the lowest PP crystalline contents in agreement with the chemical structure of this modifier and its higher needs of available interfacial volume than the aPP-SA. A second heating and pressure-free process yields PP crystalline contents very close to those of the previous cooling one but slightly above them as usual in the dynamic thermal behavior of the PP [33, 36] up to aPP-SA amounts above the optimum of the nine percent. It informs about a well-processed material with minimized reordering processes across the dynamic amorphous/crystal interphase in the bulk of each homopolymer domain in the blend [58, 77–81].

The evolution plots of the PA6 crystalline content, coming from the same cooling and pressure-free process, look very different from those of the PP ones. The lowest aPP-SA amounts show around thirty percent of decrease in the PA6 crystalline contents with respect to those in the compression-molded modified blends, approaching these as the aPP-SA amount increases. Meanwhile the aPP-SF/SA modified blends evolve as an almost slope zero straight line yielding values very close to the PA6 crystalline content values in the compression-molded modified blends, up to the 9% in aPP-SF/SA. Above this amount, increasing contents of aPP-SF/SA make the almost constant PA6 crystalline content hold off those in the compression-molded modified blend. Moreover, the PA6 crystalline content of the subsequent heating and pressure-free process shows its lowest and almost constant values just above the 9% for the aPP-SA modified blends and just below it for the aPP-SF/SA modified ones. It agrees with the proposed saturation effect of the aPP-SF/SA that induces its highest restriction effect over the PA6 crystalline content just at its lowest amounts and yielding in fact almost the same values as those found for the highest aPP-SA amounts.

It is interesting to observe the different effect of any of both interfacial modifiers on the overall crystalline content of each of both homopolymers on the compression-molded modified fifty/fifty blends. While the crystalline content of the PP decreases as the interfacial modifier amount increases, the PA6 crystalline content remains always constant in the modified blends up to the 9% of any of both interfacial modifiers, increasing slightly hereinafter. Moreover, the decrease in the PP crystalline content shows a clearly defined minimum at 9% of any of both interfacial agents, increasing slightly from this point as the interfacial agent amount increases as the PA6 crystalline content does. These findings correlate well with the previously discussed microscopy and mechanical results because also by the DSC technique one finds the optimum amount of the interfacial modifier based on the available interfacial volume and independently of its structure.

To correlate with the tensile test results we come back to the PP and the PA6 crystalline contents from the first heating scans displayed in Figure 11 but now discussed in terms of the amorphous/crystal ratio (ACR) [77, 78]. The critical point of 9 percent identifies the minimum crystalline content and then the maximum of the ACR, whatever the interfacial modifier on either the PP or the PA6 phases. As mentioned above, the effect of the interfacial modifiers is the most sensitive over the PP phase without chemical reaction possibilities with any of them. Figure 12 shows both the tensile strength and tensile strain evolution plots, both referring to the overall amorphous phase unit as previously defined.

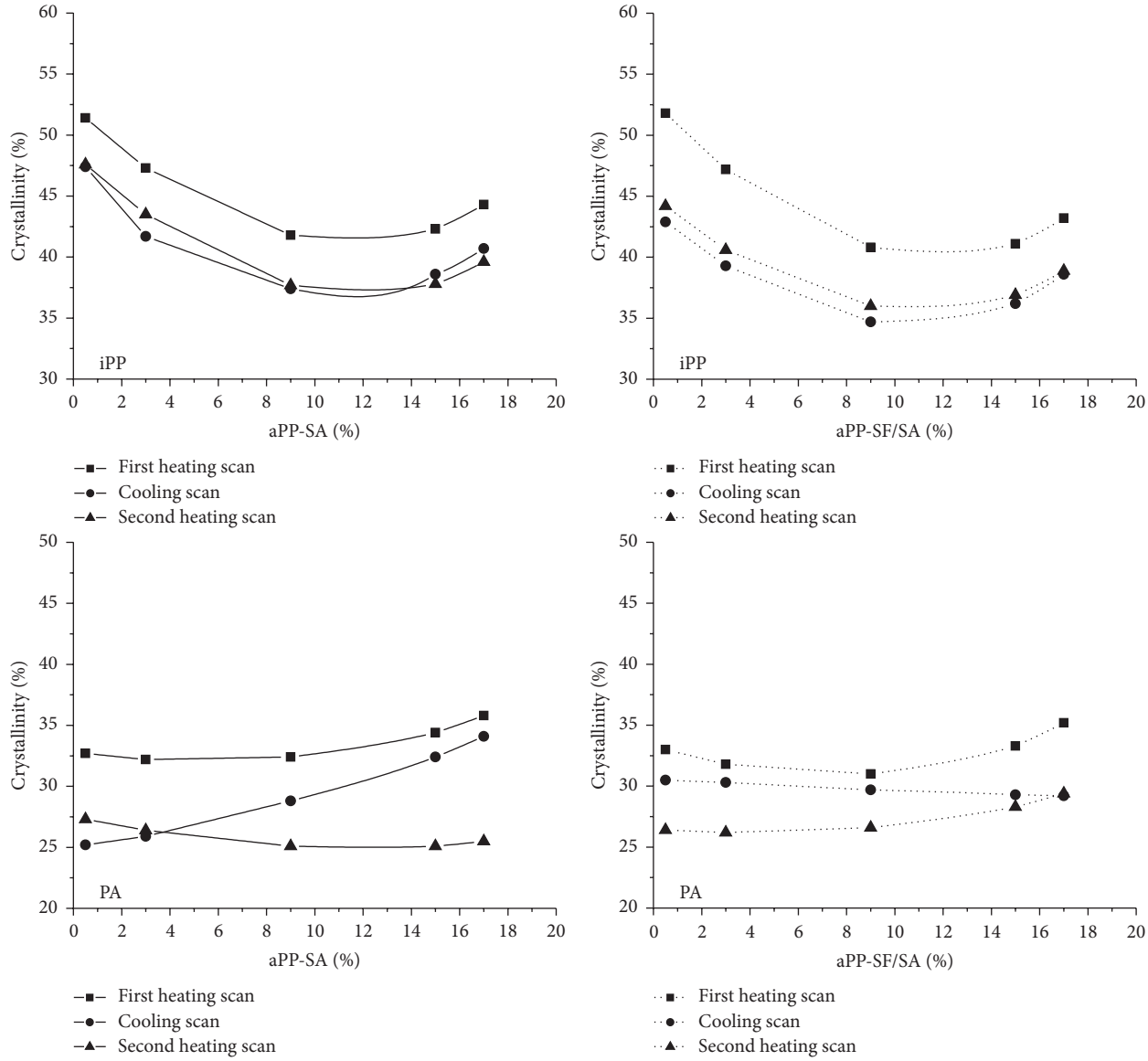

Figure 11: Crystalline content of Box-Wilson forecasts for PP (top plots) and PA6 in aPP-SA or aPP-SF/SA modified PP/PA6 fifty/fifty blends.

In terms of mechanical strength and over the specific tensile strength plot, one finds the maximum value reached at the optimum of 9% almost matching both the yield and the break strength values referring to the amorphous phase unit at this optimum of 9% and whatever the interfacial modifier. Below the optimum, the aPP-SF/SA modifier shows its saturation effect by the increase in its specific tensile strength values with respect to the pristine blend. It looks as just the opposite behavior shown by the aPP-SA one, with the lowest yield and break strength values referring to the amorphous phase unit, even below those of the pristine blend.

Over the yield and break tensile strain values referring to the amorphous phase unit, the corresponding plots displayed in Figure 12 show very similar evolutions in their respective numerical ranges. As expected and as a first observation one may appreciate that the specific break strain values are higher than their corresponding specific yield strain values for both the aPP-SA and the aPP-SF/SA modified systems. The optimum amount of the 9% blends with the highest mechanical strength shows the closest approach between the break and the yield strain values, whatever the modifier agent. Furthermore, it is interesting to observe the almost constant break strength values referring to the amorphous phase unit given by the aPP-SA modifier agent up to the optimum of 9% with a slight increase above it. The aPP-SF/SA modified blends show the same behavior but in the specific yield strain plot, up to 9%, which is in agreement with the saturation effect. Above the optimum, the specific yield strain values decrease; meanwhile the break strain ones increase. These comments seem in excellent agreement with the two- or three-arm interfacial copolymer formed in, respectively, aPP-SA or aPP-SF/SA modified blends and with their expected inverted effects between the yield and the break stages of the tensile test.

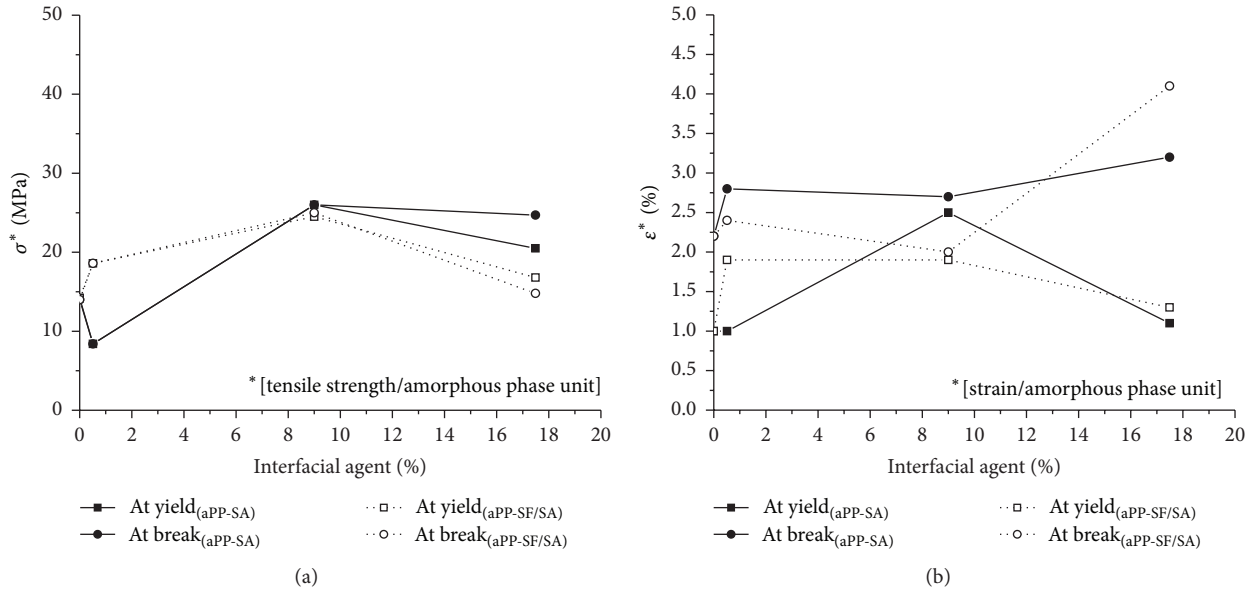

Figure 12: Experimental tensile test parameters of aPP-SA or aPP-SF/SA modified PP/PA6 fifty/fifty blends referred to the unity of overall amorphous phase.

4. Conclusions

The present paper has shown the wide spectrum of available morphologies at confined flow conditions in a well-processed fifty/fifty PP/PA6 binary system as a function not only of the amount of the interfacial modifier used but also of its structure. Indeed, the positive phase contrast transmission optical, P PC TOM, and field emission scanning electronic microscopy, FE SEM, of the different emerging morphologies from the compression-molded PP/PA6 fifty/fifty pristine and modified blends show an excellent correlation with their mechanical and dynamic thermal behavior.

The study reveals that, beyond the interfacial tension reduction between the PP and the PA6 domains, each of both interfacial modifiers gives rise to "microbridges" on selected sites of the interphase. It is consistent with the primary bonds formation between the PA6 end amine groups and the steric hindrance of each kind of SA group grafted to each one of both interfacial agents as the FT-IR analysis reveals.

The sharp differences between the capabilities of both aPP-SA and aPP-SF/SA modified atactic polypropylenes as interfacial modifiers of the fifty/fifty PP/PA6 binary system as well as their correlation with the structural differences between each of both interfacial modifiers have been revealed. In particular, the aPP-SA, 9%, modified blend yields an optimal fine grain based morphology showing the best mechanical performance of all the modified fifty/fifty blends.

The fruitful coupling between techniques of statistical design of experiments and efficient interfacial modifiers and the study of the flow-induced morphologies appear as a key parameter on the preparation of optimized polymer blends with stable morphologies. A statistically significant morphology/processing/properties relationship in incoming papers extended to the overall compositional range of the PP/PA6 binary system once fitted by following the Box-Wilson methodology lets us build up the full morphology maps for each compositional ratio and each of interfacial modifiers to tailor-make any desired blend morphology.

Conflict of Interests

The authors declare that there is no conflict of interests regarding the publication of this paper.

Acknowledgment

CICYT Research Materials Project MAT 2000-1499 financed a part of this work under the responsibility of the CSIC/ICTP/Polymer Engineering Group.

References

[1] H. Pernot, M. Baumert, F. Court, and L. Leibler, "Design and properties of co-continuous nanostructured polymers by reactive blending," *Nature Materials*, vol. 1, no. 1, pp. 54–58, 2002.

[2] P. G. de Gennes, "Conformations of polymers attached to an interface," *Macromolecules*, vol. 13, no. 5, pp. 1069–1075, 1980.

[3] J. M. García-Martínez, S. Areso, J. Taranco, and E. P. Collar, "Heterogeneous materials based on polypropylene," in *Polyolefin Blends*, T. Kyu and D. Nwabunma, Eds., chapter 13, pp. 379–410, John Wiley & Sons, Hoboken, NJ, USA, 2008.

[4] L. A. Utracki, *Polymer Alloys and Blends*, Hanser, Munich, Germany, 1989.

[5] S. Tonzani, "The renaissance of polyolefins," *Journal of Applied Polymer Science*, vol. 127, no. 2, p. 837, 2013.

[6] N. Anjum, S. K. H. Gulrez, H. Singh, and B. Gupta, "Development of antimicrobial polypropylene sutures by graft polymerization. I. Influence of grafting conditions and characterization,"

Journal of Applied Polymer Science, vol. 101, no. 6, pp. 3895–3901, 2006.

[7] R. Toth, M. Ferrone, S. Miertus, E. Chiellini, M. Fermeglia, and S. Pricl, "Structure and energetics of biocompatible polymer nanocomposite systems: a molecular dynamics study," *Biomacromolecules*, vol. 7, no. 6, pp. 1714–1719, 2006.

[8] B. C. Poon, S. P. Chum, A. Hiltner, and E. Baer, "Modifying adhesion of linear low-density polyethylene to polypropylene by blending with a homogeneous ethylene copolymer," *Journal of Applied Polymer Science*, vol. 92, no. 1, pp. 109–115, 2004.

[9] B. C. Poon, S. P. Chum, A. Hiltner, and E. Baer, "Adhesion of polyethylene blends to polypropylene," *Polymer*, vol. 45, no. 3, pp. 893–903, 2004.

[10] A. Hiltner, R. Y. F. Liu, Y. S. Hu, and E. Baer, "Oxygen transport as a solid-state structure probe for polymeric materials: a review," *Journal of Polymer Science Part B: Polymer Physics*, vol. 43, no. 9, pp. 1047–1063, 2005.

[11] D. Jarus, A. Hiltner, and E. Baer, "Barrier properties of polypropylene/polyamide blends produced by microlayer coextrusion," *Polymer*, vol. 43, no. 8, pp. 2401–2408, 2002.

[12] B. N. Jang, M. Costache, and C. A. Wilkie, "The relationship between thermal degradation behavior of polymer and the fire retardancy of polymer/clay nanocomposites," *Polymer*, vol. 46, no. 24, pp. 10678–10687, 2005.

[13] P. Song, Y. Shen, B. Du, M. Peng, L. Shen, and Z. Fang, "Effects of reactive compatibilization on the morphological, thermal, mechanical, and rheological properties of intumescent flame-retardant polypropylene," *Applied Materials & Interfaces*, vol. 1, no. 2, pp. 452–459, 2009.

[14] S. M. Lomakin, G. E. Zaikov, and E. V. Koverzanova, "Thermal degradation and combustibility of polypropylene filled with magnesium hydroxide micro-filler and polypropylene nano-filled aluminosilicate composite," *Oxidation Communications*, vol. 28, no. 2, pp. 451–464, 2005.

[15] V. Abetz, T. Brinkmann, M. Dijkstra et al., "Developments in membrane research: from material via process design to industrial application," *Advanced Engineering Materials*, vol. 8, no. 5, pp. 328–358, 2006.

[16] H. Presting and U. König, "Future nanotechnology developments for automotive applications," *Materials Science and Engineering C*, vol. 23, no. 6–8, pp. 737–741, 2003.

[17] P. Galli and G. Vecellio, "Polyolefins: the most promising large-volume materials for the 21st century," *Journal of Polymer Science, Part A: Polymer Chemistry*, vol. 42, no. 3, pp. 396–415, 2004.

[18] F. Gardiner, *Plastics and Environment*, Smithers Rapra, Shrewsbury, UK, 2010.

[19] M. Gahleitner, "Polyolefins for the 21st century," *eXPRESS Polymer Letters*, vol. 5, no. 11, p. 936, 2011.

[20] E. P. Collar and J. M. García-Martínez, "On chemical modified polyolefins by grafting of polar monomers. A survey based on recent patents literature," *Recent Patents on Materials Science*, vol. 3, no. 1, pp. 76–91, 2010.

[21] J. F. Joanny, "Polymers at interfaces," *Interface Science*, vol. 11, no. 2, pp. 157–158, 2003.

[22] J. Huang, I. Ichinose, and T. Kunitake, "Nanocoating of natural cellulose fibers with conjugated polymer: hierarchical polypyrrole composite materials," *Chemical Communications*, no. 13, pp. 1717–1719, 2005.

[23] K. P. Chong, "Nanoscience and engineering in mechanics and materials," *Journal of Physics and Chemistry of Solids*, vol. 65, no. 8-9, pp. 1501–1506, 2004.

[24] S. S. Ray and M. Okamoto, "Polymer/layered silicate nanocomposites: a review from preparation to processing," *Progress in Polymer Science*, vol. 28, no. 11, pp. 1539–1641, 2003.

[25] G. Allegra, G. Raos, and M. Vacatello, "Theories and simulations of polymer-based nanocomposites: from chain statistics to reinforcement," *Progress in Polymer Science*, vol. 33, no. 7, pp. 683–731, 2008.

[26] L. Ruiz-Pérez, G. J. Royston, J. P. A. Fairclough, and A. J. Ryan, "Toughening by nanostructure," *Polymer*, vol. 49, no. 21, pp. 4475–4488, 2008.

[27] J. M. García-Martínez, J. Taranco, O. Laguna, and E. P. Collar, "Modification of polypropylene by maleic anhydride: study on the reaction conditions using a Batch process," *International Polymer Processing*, vol. 9, no. 3, pp. 246–251, 1994.

[28] J. M. G. Martínez, J. Taranco, O. Laguna, and E. P. Collar, "Functionalization of polypropylene with maleic anhydride by reactive extrusion," *International Polymer Processing*, vol. 9, no. 4, pp. 346–349, 1994.

[29] J. M. García Martínez, O. Laguna, and E. P. Collar, "Batch process modification of atactic polypropylene by maleic anhydride in the melt. The role of reaction time," *Journal of Applied Polymer Science*, vol. 65, no. 7, pp. 1333–1347, 1997.

[30] J. M. García-Martínez, O. Laguna, and E. P. Collar, "Chemical modification of polypropylenes by maleic anhydride: influence of stereospecificity and process conditions," *Journal of Applied Polymer Science*, vol. 68, no. 3, pp. 483–495, 1998.

[31] J. M. García-Martínez, S. Areso, O. Laguna, and E. P. Collar, "Functionalization of atactic polypropylene by succinyl-fluorescein: a two-step process of chemical modification in the melt," *Journal of Applied Polymer Science*, vol. 70, no. 4, pp. 689–696, 1998.

[32] J. M. García-Martínez, A. G. Cofrades, S. Areso, O. Laguna, and E. P. Collar, "Grafting of p-phenylen-bis-maleamic acid into polypropylene in melt," *Journal of Applied Polymer Science*, vol. 69, no. 5, pp. 931–940, 1998.

[33] J. M. García-Martínez, A. G. Cofrades, O. Laguna, S. Areso, and E. P. Collar, "Influence of reactant concentration and reaction time in the chemical modification process of polypropylene by *p*-phenylen-bis-maleamic acid in the melt," *European Polymer Journal*, vol. 36, no. 10, pp. 2253–2263, 2000.

[34] J. M. García Martínez, S. Areso, and E. P. Collar, "The transient nature of maximum maleic anhydride grafting on polypropylene. A mechanistic approach based on a consecutive reaction model. I. Batch solution process," *Journal of Applied Polymer Science*, vol. 102, pp. 1182–1190, 2006.

[35] J. M. García-Martínez, S. Areso, and E. P. Collar, "The transient nature of maximum maleic anhydride grafting of polypropylene: A mechanistic approach based on a consecutive reaction model. II. A comparison of the batch solution and molten state processes," *Journal of Applied Polymer Science*, vol. 104, no. 1, pp. 345–351, 2007.

[36] E. P. Collar, S. Areso, O. Laguna, and J. M. García-Martínez, "On the thermal behaviour under dynamical conditions of succinic anhydride grafted polyolefins. A study from the crystalline regions," *European Polymer Journal*, vol. 35, no. 10, pp. 1861–1874, 1999.

[37] J. M. García-Martínez, S. Areso, O. Laguna, and E. P. Collar, "FTIR quantitative characterization of chemically modified polypropylenes containing succinic grafted groups," *Journal of Applied Polymer Science*, vol. 73, no. 14, pp. 2837–2847, 1999.

[38] J. M. García-Martínez, S. Areso, O. Laguna, E. P. Collar, and C. Marco, "On the changes in glass transition temperatures of

atactic polypropylenes induced by grafting of polar groups," *Journal of Thermal Analysis and Calorimetry*, vol. 58, no. 3, pp. 541–550, 1999.

[39] J. M. García-Martínez, S. Areso, and E. P. Collar, "Structure development of PP/PA6 blends. Interfacial modifications and preliminary modeling of macroscopic properties," *Journal of Macromolecular Science Part B: Physics*, vol. 40, no. 3-4, pp. 387–404, 2001.

[40] E. P. Collar, C. Marco, S. Areso, and J. M. García-Martínez, "Thermal behavior of PP/PA6 blends under dynamic conditions. The effect of different interfacial agents based on chemically modified atactic polypropylene," *Journal of Macromolecular Science. Part B: Physics*, vol. 40, no. 3-4, pp. 369–385, 2001.

[41] C. Marco, E. P. Collar, S. Areso, and J. M. García-Martínez, "Thermal studies on polypropylene/polyamide-6 blends modified by succinic anhydride and succinyl fluorescein grafted polypropylenes," *Journal of Polymer Science Part B: Polymer Physics*, vol. 40, no. 13, pp. 1307–1315, 2002.

[42] J. M. García Martínez, S. Areso, M. A. Gómez, C. Marco, and E. P. Collar, "Role of succinic anhydride grafted atactic polypropylene (a-PP-SA) on the melting and crystallization behaviour under dynamic conditions of the PP phase in interfacial modified polypropylene/polyamide 6 blends. A synchrotron WAXS and SAXS study," in *Hasylab Annual Report*, part I, pp. 845–846, 2002.

[43] J. M. García-Martínez, S. Areso, M. A. Gómez, C. Marco, and E. P. Collar, "On the changes of the PP phase in interfacial modified PP/PA6 by means of succinic anhydride or succinil-fluoresceine/succinic anhydride grafted atactic polypropylenes. A synchrotron WAXS and SAXS comparative study," Hasylab Annual Report Part II, 2003.

[44] B. O'Shaughnessy and U. Sawhney, "Reaction kinetics at polymer-polymer interfaces," *Macromolecules*, vol. 29, no. 22, pp. 7230–7239, 1996.

[45] B. O'Shaughnessy and D. Vavylonis, "Irreversibility and polymer adsorption," *Physical Review Letters*, vol. 90, no. 5, Article ID 056103, 2003.

[46] O. Sadiku-Agboola, E. R. Sadiku, A. T. Adegbola, and O. F. Biotidara, "Rheological properties of polymers: structure and morphology of molten polymer blends," *Materials Sciences and Applications*, vol. 02, no. 01, pp. 30–41, 2011.

[47] P. Van Puyvelde, A. Vananroye, R. Cardinaels, and P. Moldenaers, "Review on morphology development of immiscible blends in confined shear flow," *Polymer*, vol. 49, no. 25, pp. 5363–5372, 2008.

[48] A. Ajji and L. A. Utracki, "Interphase and compatibilization of polymer blends," *Polymer Engineering and Science*, vol. 36, no. 12, pp. 1574–1585, 1996.

[49] M. Gahleitner, "Melt rheology of polyolefins," *Progress in Polymer Science*, vol. 26, no. 6, pp. 895–944, 2001.

[50] I. Duvall, C. Sellitti, C. Myers, A. Hilters, and E. Baer, "Effect of compatibilization on the properties of polypropylene/polyamide-66 (75/25 wt/wt) blends," *Journal of Applied Polymer Science*, vol. 52, no. 2, pp. 195–206, 1994.

[51] V. V. Ginzburg, G. Peng, F. Qiu, D. Jasnow, and A. C. Balazs, "Kinetic model of phase separation in binary mixtures with hard mobile impurities," *Physical Review E*, vol. 60, no. 4, pp. 4352–4359, 1999.

[52] P. T. Hietaoja, R. M. Holsti-Miettinen, J. V. Seppala, and O. T. Ikkala, "The effect of viscosity ratio on the phase inversion of polyamide 66/polypropylene blends," *Journal of Applied Polymer Science*, vol. 54, no. 11, pp. 1613–1623, 1994.

[53] M. Gabriele, R. Pasquino, and N. Grizzuti, "Effects of viscosity-controlled interfacial mobility on the coalescence of immiscible polymer blends," *Macromolecular Materials and Engineering*, vol. 296, no. 3-4, pp. 263–269, 2011.

[54] A. González-Montiel, H. Keskkula, and D. R. Paul, "Morphology of nylon 6/polypropylene blends compatibilized with maleated polypropylene," *Journal of Polymer Science. Polymer Physics*, vol. 33, pp. 1751–1767, 1995.

[55] B. Minisini and F. Tsobnang, "Molecular dynamics study of specific interactions in grafted polypropylene organomodified clay nanocomposite," *Composites Part A: Applied Science and Manufacturing*, vol. 36, no. 4, pp. 539–544, 2005.

[56] M. H. Cheng, A. C. Balazs, C. Yeung, and V. V. Ginzburg, "Modeling reactive compatibilization of a binary blend with interacting particles," *The Journal of Chemical Physics*, vol. 118, no. 19, pp. 9044–9052, 2003.

[57] F. Ciardelli, S. Coiai, E. Passaglia, A. Pucci, and G. Ruggeri, "Nanocomposites based on polyolefins and functional thermoplastic materials," *Polymer International*, vol. 57, no. 6, pp. 805–836, 2008.

[58] Q. H. Zeng, A. B. Yu, and G. Q. Lu, "Multiscale modeling and simulation of polymer nanocomposites," *Progress in Polymer Science*, vol. 33, no. 2, pp. 191–269, 2008.

[59] P. Van Puyvelde, Z. Oommen, P. Koets, G. Groeninckx, and P. Moldenaers, "Effect of reactive compatibilization on the interfacial slip in nylon-6/EPR blends," *Polymer Engineering and Science*, vol. 43, no. 1, pp. 71–77, 2003.

[60] D. Shi, Z. Ke, J. Yang, Y. Gao, J. Wu, and J. Yin, "Rheology and morphology of reactively compatibilized PP/PA6 blends," *Macromolecules*, vol. 35, no. 21, pp. 8005–8012, 2002.

[61] O. Sadiku-Agboola, E. R. Sadiku, A. T. Adegbola, and O. F. Biotidara, "Rheological properties of polymers: structure and morphology of molten polymer blends," *Materials Sciences and Applications*, vol. 2, no. 1, pp. 30–41, 2011.

[62] C. Verdier, H. T. M. Vinagre, M. Piau, and D. D. Joseph, "High temperature interfacial tension measurements of PA6/PP interfaces compatibilized with copolymers using a spinning drop tensiometer," *Polymer*, vol. 41, no. 17, pp. 6683–6689, 2000.

[63] R. Cardinaels, A. Vananroye, P. Van Puyvelde, and P. Moldenaers, "Breakup criteria for confined droplets: effects of compatibilization and component viscoelasticity," *Macromolecular Materials and Engineering*, vol. 296, no. 3-4, pp. 214–222, 2011.

[64] G. E. P. Box, W. G. Hunter, and J. S. Hunter, *Statistics for Experimenters*, John Wiley & Sons, New York, NY, USA, 1978.

[65] J. E. Mark, *Physical Properties of Polymer Handbook*, Springer, New York, NY, USA, 2nd edition, 2007.

[66] D. A. Hemsley, *Applied light Microscopy*, Elsevier, New York, NY, USA, 1989.

[67] D. B. Murphy, *Fundamentals of Light Microscopy and Electronic Imaging*, Wiley, New York, NY, USA, 2001.

[68] J. Bodensohn and W. I. Goldburg, "Spinodal decomposition between closely spaced plates," *Physical Review A*, vol. 46, no. 8, pp. 5084–5088, 1992.

[69] H. Tanaka, "Wetting dynamics in a confined symmetric binary mixture undergoing phase separation," *Physical Review Letters*, vol. 70, no. 18, pp. 2770–2773, 1993.

[70] H. Hoppe, M. Heuberger, and J. Klein, "Self-similarity and pattern selection in the roughening of binary liquid films," *Physical Review Letters*, vol. 86, no. 21, pp. 4863–4866, 2001.

[71] C. Cerclé and B. D. Favis, "Generalizing interfacial modification in polymer blends," *Polymer*, vol. 53, no. 20, pp. 4338–4343, 2012.

[72] J. Baschnagel, H. Meyer, F. Varnik et al., "Computer simulations of polymers close to solid interfaces: some selected topics," *Interface Science*, vol. 11, no. 2, pp. 159–173, 2003.

[73] I. Kolesov, O. Dolynchuk, S. Borreck, and H.-J. Radusch, "Morphology-controlled multiple one- and two-way shape-memory behavior of cross-linked polyethylene/poly(ε-caprolactone) blends," *Polymers for Advanced Technologies*, vol. 25, no. 11, pp. 1315–1322, 2014.

[74] M. A. Carignano and I. Szleifer, "Controlling surface interactions with grafted polymers," *Interface Science*, vol. 11, no. 2, pp. 187–197, 2003.

[75] L. Engel, H. Kliengele, G. W. Ehrenstein, and H. Schaper, *An Atlas of Polymer Damage*, Hanser, Munich, Germany, 1981.

[76] J. Karger-Kocsis, *Polypropylene: Structure, Blends and Composites*, Chapman Hall, New York, NY, USA, 1995.

[77] I. Duvall, C. Sellitti, C. Myers, A. Hiltner, and E. Baer, "Interfacial effects produced by crystallization of polypropylene with polypropylene-*g*-maleic anhydride compatibilizers," *Journal of Applied Polymer Science*, vol. 52, no. 2, pp. 207–216, 1994.

[78] D. Sikdar, D. R. Katti, and K. S. Katti, "The role of interfacial interactions on the crystallinity and nanomechanical properties of clay—polymer nanocomposites: a molecular dynamics study," *Journal of Applied Polymer Science*, vol. 107, no. 5, pp. 3137–3148, 2008.

[79] A. Sacchi, L. Di Landro, M. Pegoraro, and F. Severini, "Morphology of isotactic polypropylene-polyamide 66 blends and their mechanical properties," *European Polymer Journal*, vol. 40, no. 8, pp. 1705–1713, 2004.

[80] E. P. Collar, S. Areso, and J. M. García-Martínez, "Interfacial modifications on the PP/PA6, fifty/fifty blend, as synchrotron and DMA revealed," Polymer Engineering Group' Results, 2013.

[81] P. J. Lemstra, "Confined polymers crystallize," *Science*, vol. 323, no. 5915, pp. 725–726, 2009.